Nucleic Acids Research, 2023, **51**, 12242–12260
https://doi.org/10.1093/nar/gkad967
Advance access publication date: 1 November 2023
Genome integrity, repair and replication

The RNA-binding motif protein 14 regulates telomere integrity at the interface of TERRA and telomeric R-loops

Yajun Wang[1,2], Wei Zhu[1], Yumi Jang[3], Joshua A. Sommers[4], Gong Yi[1], Chandrakala Puligilla[1], Deborah L. Croteau[1], Yibin Yang[2], Mihoko Kai[3] and Yie Liu[1,*]

[1]Laboratory of Genetics and Genomics, 251 Bayview Blvd, National Institute on Aging/National Institutes of Health, Baltimore, MD 21224, USA
[2]Blood Cell Development and Function Program, Fox Chase Cancer Center, Philadelphia, PA 19111, USA
[3]Department of Radiation Oncology and Molecular Radiation Sciences, Johns Hopkins University School of Medicine, Baltimore, MD 21287, USA
[4]Translational Gerontology Branch, 251 Bayview Blvd, National Institute on Aging/National Institutes of Health, Baltimore, MD 21224, USA
*To whom correspondence should be addressed. Tel: +1 410 454 8633; Fax: +1 410 558 8157; Email: liuyie@nih.gov

Abstract

Telomeric repeat-containing RNA (TERRA) and its formation of RNA:DNA hybrids (or TERRA R-loops), influence telomere maintenance, particularly in human cancer cells that use homologous recombination-mediated alternative lengthening of telomeres. Here, we report that the RNA-binding motif protein 14 (RBM14) is associated with telomeres in human cancer cells. RBM14 negatively regulates TERRA expression. It also binds to TERRA and inhibits it from forming TERRA R-loops at telomeres. RBM14 depletion has several effects, including elevated TERRA levels, telomeric R-loops, telomere dysfunction-induced DNA damage foci formation, particularly in the presence of DNA replication stress, pRPA32 accumulation at telomeres and telomere signal-free ends. Thus, RBM14 protects telomere integrity via modulating TERRA levels and its R-loop formation at telomeres.

Graphical abstract

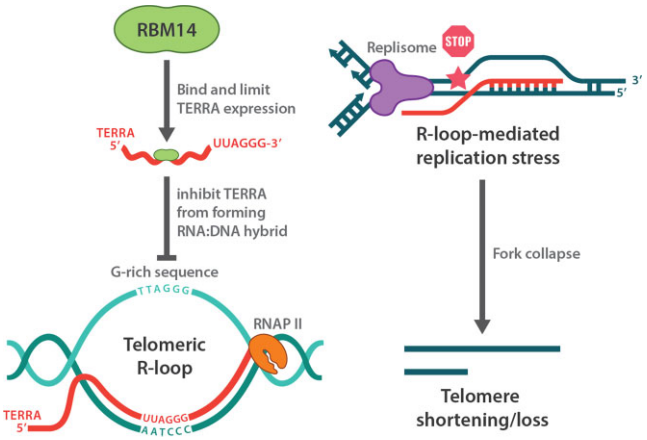

Introduction

Telomeres are chromosome termini structures consisting of tandem DNA nucleotide repeats and the shelterin protein complex, including the telomeric repeat-binding factors 1 (TRF1) and 2 (TRF2)(1). Telomeres protect chromosome ends from degradation and being recognized as damaged DNA, and telomere dysfunction due to loss of telomeric DNA repeats or loss of protection by the shelterin complex leads to the DNA damage response, resulting in cell growth retardation, cellular senescence, or apoptosis (1–3). Telomeres are typically maintained by telomerase in human cancer cells, whereas 10–15% of human cancer cells use homologous recombination (HR)-mediated 'alternative lengthening of telomeres' (ALT) to maintain telomere length (4–7). Additionally, telomere repeats have a natural inclination to produce branching nucleotide intermediates, which presents an inherent obstacle to telomere replication and consequently impacts telomere maintenance (8,9).

TERRA has been found in a variety of species, including humans (10–15). TERRA is transcribed from subtelomeric to telomeric regions by RNA polymerase II, and it is crucial for telomere preservation (11,12,16–19). Because of its guanine-rich sequence composition, TERRA has a propensity to form an RNA:DNA hybrid with the cytosine-rich telomeric DNA strand. As a result, the telomeric strand containing the TTAGGG repeats shifts, resulting in the formation of

Received: February 9, 2023. **Editorial Decision:** October 3, 2023. **Accepted:** October 13, 2023

an R-loop structure (20,21). Mounting evidence suggests that TERRA R-loop formation is crucial for telomere maintenance (20,22,23); however, excessive TERRA R-loops may interfere with DNA replication, causing replication stress, chromosomal fragility or rearrangements and telomere loss (21,23–25).

TERRA and TERRA R-loops are highly abundant in ALT human cancer cells (20,21,26). TERRA R-loops are closely controlled in eukaryotic telomeres (21). RNase H1 has been shown to localize to the ALT telomere, where it degrades TERRA in the RNA:DNA duplex and antagonizes R-loop formation (20). RNase H1 depletion increased R-loop formation, causing replication stress and telomere fragility (20). TERRA transcripts are bound by a complex array of factors, which could also impact TERRA levels and TERRA R-loop formation. Notably, the key telomeric protein TRF2 binds to TERRA via its N-terminal RNA-binding GAR domain and stimulates telomeric R-loop formation (27–29). Deletion of the TRF2 GAR domain results in telomere dysfunction via loss of TERRA (28).

A recent proteomic screening has identified an association between the RNA-Binding Motif Protein 14 (RBM14) and TERRA (30). RBM14 has a role in the repair of double-strand DNA breaks (DSBs) through a process called non-homologous end joining (NHEJ) (31–33). Furthermore, it has been established that RBM14 possesses two RNA recognition motifs (RRMs), engages in interactions with genome R-loops and exerts regulatory control on RNA transcription and splicing processes (31,34,35). It has been shown that, aside from its well-known role in DSB repair, BRCA1 engages in direct interactions with TERRA and facilitates the resolution of TERRA R-loops. This procedure ensures the presence of an appropriate amount of TERRA R-loops at telomeres, thereby mitigating telomere replication stress induced by an excessive accumulation of TERRA R-loops (36). Thus, we set out to investigate the role of RBM14 in the regulation of TERRA and TERRA R-loops and its consequent impact on telomere maintenance in human cancer cells, with a focus on ALT cancer cells. Our findings revealed that RBM14 is involved in telomeric chromatin and modulates TERRA levels and the formation of TERRA R-loops at telomeres, which contributes to the preservation of telomere integrity in human cancer cells.

Materials and methods

Plasmids, siRNAs, antibodies, western blots and cell lines

GFP-RBM14 was a gift from Dr. Lan Ko, Medical College of Georgia, Augusta, GA. The RNAi-resistant GFP-RBM14 plasmid was generated by mutating one codon in the siRNA RBM14 targeted region from 'atcgcgcagctcaacggcaaa' to 'atcgcgcagctaaacggcaaa' in GFP-RBM14. GFP-RNase H1 was obtained from Addgene (plasmid #108699). The small interfering RNA (siRNA) RBM14 #1 (siRBM14$^{\#1}$)(SI03048374) and non-targeting control (siNT)(SI03650318) were acquired from Qiagen, while siRNA RBM14 #2 (siRBM14$^{\#2}$)(SC-96838) was purchased from Santa Cruz. All siRNAs were transfected with Lipofectamine RNAiMAX (Thermo Fisher Scientific, 13778). TERRA knockdown was performed as described previously (30). Cells were transfected with the TERRA antisense (TAACCCTAACCCTAAC) or non-targeting control (ACCTACCTCAATACCA) LNA gapmers (Qiagen/Exiqon, #339511) at a concentration of 2–8 μM in 100 μl nucleofector solution using the A30 program (nucleofector kits, Lonza).

RBM14 knockdown and RNAi-resistant GFP-RBM14 expression were confirmed by western blotting. Cells were harvested and extracted in RIPA buffer (Thermo Scientific, 89901) supplemented with a protease inhibitor cocktail (Thermo Scientific, 78442). The protein samples were separated by Bis-Tris gel and transferred to a nitrocellulose membrane. The blot was detected using the primary antibodies. Images were examined using a Femto chemiluminescence substrate kit (Thermo Scientific, 34094), captured with Image Lab software (Bio-Rad) and analyzed with Quantity One (Bio-Rad) software. Protein levels are normalized to GAPDH.

Primary antibodies used in this study are provided in Supplementary Table S1. These antibodies include RBM14 (Abcam, ab70636), TRF1 (Abcam, ab10579), 53BP1 (Novus Biological, NB100-304), DNA-RNA Hybrid (S9.6)(Kerafast, ENH001), RPA32/RPA2 (phospho S33) (Abcam, ab211877), TRF2 (Novus Biological, NB100-56506 and Thermo Scientific, MA1-41001), PML (Santa Cruz, sc-9862) and GAPDH (Abcam, ab22555).

Cells were cultivated in Dulbecco's Modified Eagle Medium supplemented with 20% bovine calf serum and antibiotics at 37°C in a 5% CO_2 incubator. Cells were treated with 1 μM Olaparib and 2 μM STL127705 [MedChemExpress, AZD2281 (KU-0059436) and HY-122727], respectively, for 24 h before being harvested for ChIP analysis.

ChIP assays

ChIP was performed as previously described (37). Briefly, cells were crosslinked with 1% formaldehyde in culture media for 10 min before being quenched with 125 mM glycine. Cells were then permeabilized with swelling buffer (5 mM PIPES, pH 8.0, 85 mM KCl, 0.5% NP-40). Nuclei were resuspended in MNase digestion buffer (10 mM Tris, pH 7.4, 15 mM NaCl, 60 mM KCl, 0.15 mM spermine, 0.5 mM spermidine) and incubated with 0.8 U MNase (Thermo Scientific) for 30–45 min at 37°C. The reaction was stopped by adding 50 mM EDTA, followed by centrifugation. The nuclear pellets were resuspended in 10 mM Tris–HCl (pH 8.0), 100 mM NaCl, 1 mM EDTA, 0.5 mM EGTA, 0.1% Na-deoxycholate and 0.5% *N*-lauroylsarcosine. Lysates were sonicated briefly to disrupt nuclear membranes using an ultrasonicator (settings: 30 s 'ON'/30 s 'OFF'; power: 'High'; time: 5 min) with a water bath (Bioruptor, Diagenode). After the addition of 1% Triton X-100, diluted lysates were incubated overnight at 4°C with the antibodies. Protein A/G PLUS-Agarose beads (Santa Cruz Biotechnology, 10% v/v) were used for immunoprecipitations.

To detect RBM14 and telomeric R-loop association, ChIP-reChIP was performed as previously described (38). Following nuclear sonication, lysates were diluted and incubated overnight at 4°C with constant rotation with 5 μg of RBM14 antibody. Each sample was incubated with 50 μl of preabsorbed beads at 4°C for 2–4 h and washed sequentially with 1 ml of washing buffers I (0.1% SDS, 1% Triton X-100, 2 mM EDTA, 150 mM NaCl, 20 mM Tris–HCl, pH 8.1), washing buffers II (0.1% SDS, 1% Triton X-100, 2 mM EDTA, 500 mM NaCl, 20 mM Tris–HCl, pH 8.1) and washing buffers III (0.25 M LiCl, 1% NP40, 1% Deoxycholate, 1 mM EDTA, 10 mM Tris–HCl, pH 8.1) with rotation for 10 min at 4°C. All the washing buffers were supplemented with protease in-

hibitors. One minute of centrifugation at 800 g was conducted between washings. After carefully removing the supernatant with a pipette, beads were incubated in 75 μl TE buffer with 10 mM DTT for 30 min at 37°C to elute immunocomplexes. Following centrifugation at 800 g for 2 min, the supernatant was transferred into a 1.5 ml tube. The sample was diluted 20 times with dilution buffer to a final volume of 1.5 ml. Each sample was incubated with 5 μg of S9.6 antibody overnight at 4°C with constant rotation. Following binding, the beads were washed sequentially with 1 ml of washing buffers I, II and III. Each sample was incubated with 150 μl of washing beads buffer containing proteinase K and RNase A (5 μg/μl) for at least 4 h or overnight at 65°C to reverse the crosslink.

DNA extraction was performed using the QIAquick PCR Purification Kit (QIAGEN, 28104). Dot-blot analyses were employed to quantify ChIP DNA. For dot blot analyses, ChIP DNA was denatured with 0.5 M NaOH and 1.5 M NaCl, and equal volumes of samples were loaded onto an Amersham Hybond-N + membrane (GE Healthcare) using a Bio-Dot apparatus (Bio-Rad). Membranes were washed once with denaturing buffer and wash buffer (3× SSC), followed by UV-crosslinking (UV Stratalinker 2400, Stratagene) and blocked with 10× Denhardt's solution (Thermo Scientific) for 1 h at 37°C. Hybridization was conducted at 37°C overnight using either Telo-C-Biotin $(CCCTAA)_4$ or Alu (5′-Biotin-GGCCGGGCGCGGTGGCTCACGCCTGTAATCCCAGCA-3′) probes (Integrated DNA Technologies, IDT DNA). Signal detection was performed using the chemiluminescent nucleic acid detection module kit (Thermo Scientific, catalog no. 89880). Images were obtained via the ChemiDoc imager (Bio-Rad) and quantified with ImageQuant TL software (GE Healthcare Life Sciences). ChIP DNA in telomeric and subtelomeric regions was also measured using quantitative real-time PCR (qPCR). The PCR value was calculated by the $2^{-\Delta\Delta CT}$ method (39). Primer sequences utilized for PCR analysis were provided in Supplementary Table S2. Dot-blot or PCR values were subjected to normalization to the value corresponding to 100% input.

RNA preparation and analysis

Total RNA was purified with Trizol reagent (ThermoFisher) in the presence of an RNase inhibitor according to the manufacturer's instructions. In brief, the sample was mixed with 1 ml of Trizol and 200 μl of chloroform. The mixture was centrifuged at 4°C for 15 min at 12 000 g, and the aqueous phase was collected and precipitated with isopropanol in equal volume. The RNA pellets were collected by centrifugation at 12 000 g for 10 min, then washed with 75% ethanol, air-dried and resuspended in RNase-free H_2O. The sample was then treated with DNase I at 37°C for 45 min, followed by inactivation at 65°C in the presence of EDTA for 5 min.

For Northern blotting, approximately 7.5–10 μg of total RNA was denatured in loading buffer at 65°C for 15 min, separated by 1.2% agarose-formamide gel in 1× MOPS buffer, transferred to an Amersham Hybond-N^+ membrane (GE Healthcare) with 10× SSC, and crosslinked on the membranes in a UV Stratalinker 2400 (Stratagene) at 125 mJ. The membrane was hybridized with the Telo-C-Biotin $(CCCTAA)_4$ probe. TERRA levels were normalized to 18S internal control. Dot-blot was performed by loading 1 μg of total RNA per sample onto an Amersham Hybond-N^+ membrane (GE Healthcare). The membrane was hybridized with the Telo-C-Biotin $(CCCTAA)_4$ or 18S (5′-Biotin-CCATCCAATCGGTAGTAGCG-3′) probes (IDT DNA). For RNase A controls, RNA samples were treated with RNase A (QIAGEN) at a final concentration of 100 μg/ml at 37°C for 30–60 min.

Reverse transcription real-time PCR (RT-qPCR) analysis of individual TERRA was carried out as described (40). For TERRA stability analysis, cells were treated with 7.5 nM actinomycin D for 12 h. In brief, 1 μg of RNA was reverse transcribed using $(CCCTAA)_5$ oligonucleotides for TERRA or random decamers for other genes with Super Script III Reverse Transcriptase (Invitrogen). Overall, 100 ng of cDNA were analyzed by qPCR with SYBR Green. The PCR value was determined by $2^{-\Delta\Delta CT}$ methods and normalized to 18S. Primer sequences used for RT–qPCR were listed in Supplementary Table S2.

RNA immunoprecipitation (RIP)

RIP assays were performed as described (29). Cells were crosslinked with formaldehyde at a final concentration of 1% for 10 min. To stop cross-linking, glycine at a final concentration of 125 mM was added. Cells were pelleted by centrifugation at 800 g for 5 min, washed with cold 1× PBS, resuspended in 600 μl of buffer A [0.5% NP40, 5 mM PIPES, pH 8.0, 85 mM KCl, 50 U/ml SUPERase•In™ RNase Inhibitor (ThermoFisher), protease inhibitor cocktail (ThermoFisher)] and incubated on ice for 10 min. Nuclei were collected by centrifugation at 3000 g for 5 min at 4°C, washed in NP-40-free buffer A and resuspended in 600 μl of buffer B (10 mM EDTA, 50 mM Tris–HCl, pH 8.1, 1% SDS, 50 U/ml SUPERase•in™ RNase Inhibitor, protease inhibitor cocktail) for 10 min on ice. Lysates were sonicated and centrifuged at 15 000 g for 10 min at 4°C. The supernatant was collected and diluted 10-fold using IP buffer (1.1% Triton X-100, 0.01% SDS, 167 mM NaCl, 1.2 mM EDTA, 16.7 mM Tris, pH 8.1, 50 U/ml SUPERase•in™ RNase Inhibitor, protease inhibitor cocktail). An antibody (2–10 μg) was added to the reaction. The mixture was incubated for 2 h to overnight at 4°C with gentle rotation. Protein A/G beads (40 μl) were added to the mixture and subjected to incubation for 1 hour at 4°C with gentle rotation. Each IP reaction was washed five times (10 min each) in 1 ml IP buffer at 4°C and eluted at 70°C for 20 min with 200 μl elution buffer (1% SDS, 5 mM EDTA, 10 mM Tris, pH 8.0, 50 U/ml SUPERase•in™ RNase Inhibitor, protease inhibitor cocktail), and then at 70°C for 1–2 h to reverse crosslink. RNA was extracted with Trizol reagent, resuspended in 50 μl of DEPC-treated water, treated with 2 μl DNase I (2 U/μl, Thermo Fisher Scientific, AM2222) and analyzed by dot blot using the Telo-C-Biotin $(CCCTAA)_4$ or TERRA-like-Biotin $(GGGATT)_4$ probes (IDT DNA). For controls, RNA samples were treated with RNase A (QIAGEN) at a final concentration of 100 μg/ml at 37°C for 30–60 min.

Immunofluorescence (IF), proximal ligation assay (PLA) and TERRA RNA fluorescence *in situ* hybridization (TERR RNA-FISH)

IF was performed as described (41) with a few modifications. Cells were seeded and cultured on Lab-Tek II chambered glass slides (Nunc). Cells were fixed with 4% formaldehyde at 4°C, permeabilized with 0.2% Triton X-100 and blocked with 3% BSA. Cells were immunostained with primary antibodies at 4°C overnight, followed by Alexa Fluor-labeled secondary an-

tibodies (Abcam) for 1 h at 37°C. For detection of RBM14, cells were treated with the cytoskeletal (CSK) solution (100 mM NaCl, 10 mM PIPES, pH 6.8, 300 mM sucrose, 3 mM $MgCl_2$, 0.5% Triton X-100) for 5 min on ice and then 100% methanol for 10 min at –20°C, prior to blocking and immunostaining.

PLA was performed using Duolink® PLA Starter Kits (Sigma-Aldrich), following the manufacturer's guidelines with minor modifications (42). A combination between TRF2 and RBM14 antibodies was used to detect the association between RBM14 and telomeres, and a combination between TRF2 and 53BP1 antibodies was used to detect the association between 53BP1 and telomeres. For IF combined with PLA, the PLA procedure was followed by immunofluorescence staining with a secondary antibody, as described (42). Supplementary Table S1 lists primary and secondary antibody combinations for PLA procedures.

TERRA RNA-FISH was performed as described with minor modifications (10). Cells were permeabilized with cytobuffer (10 mM PIPES, pH 6.8, 100 mM NaCl, 3 mM $MgCl_2$, 300 mM sucrose), cytobuffer with 0.5% Triton-X and then cytobuffer for 30 s for each step. Cells were fixed in ice-cold 4% paraformaldehyde in 1× PBS for 10 min at room temperature and dehydrated twice in ice-cold 70% ethanol for 2 min, ice-cold 90% ethanol for 1 min and ice-cold 100% ethanol for 1 min. Slides were incubated with a Cy3-labeled $(CCCTAA)_3$ PNA probe (Panagene) in a humid chamber (2× SSC, 50% formamide) overnight at 37°C, followed by washing once in 2× SSC for 3 min at room temperature, three times in 2× SSC for 5 min at 37°C and briefly in 4× SSC. Slides were then mounted in ProLong™ Gold Antifade Mounting Solution with DAPI (ThermoFisher). For IF combined with TERRA RNA-FISH, cells were permeabilized with cytobuffer and then subjected to the immunofluorescence protocol. Following the secondary antibody washing process, cells were fixed for 2 min at room temperature with 4% paraformaldehyde, dehydrated and followed by RNA FISH.

Cells were counterstained with ProLongTM Gold Antifade Mounting Solution with DAPI (ThermoFisher). Images were captured with a fluorescence microscope (Axio2, Carl Zeiss) and scored manually. Data presentation was performed using GraphPad software. Approximately 100 cells per genotype or condition were analyzed.

Telomere length and function assessment

Telomere length was determined by telomere restriction fragment (TRF) analysis on genomic DNA and quantitative telomere *in situ* hybridization (Q-FISH) on metaphase spreads, as previously described (43). Genomic DNA was isolated from cells using a DNA isolation kit (Qiagen) and digested by AluI, MboI and RNase A. Digested DNA was separated on a 0.8% (w/v) agarose gel by electrophoresis, denatured with alkaline buffer (2.5 M NaCl, 1.5 M NaOH) and transferred to a membrane. The hybridization was performed with a Telo-C-Biotin $(CCCTAA)_4$ probe (IDT DNA). The TRF blot was visualized using a chemiluminescent nucleic acid detection module kit (Thermo Scientific, catalog no. 89880). Images were quantified using the ImageQuant TL software, and the mean telomere length was calculated using Quantity One (Bio-Rad) software. For Q-FISH analysis, cells were incubated with 0.1 μg ml^{-1} colcemid (ThermoFisher) for 2 h at 37°C, collected and immediately incubated in 75 mM KCl for 15–20 min at 37°C, fixed in ice-cold methanol and glacial acetic acid (3:1) and dropped onto glass slides. Metaphase spreads were hybridized with a Cy3-labeled $(CCCTAA)_3$ PNA probe (0.5 μg ml^{-1}, Panagene), washed and mounted with ProLongTM Gold Antifade Mounting Solution with DAPI (ThermoFisher). Images were captured using Cytovision software (Applied Imaging) on a fluorescence microscope (Axio2; Carl Zeiss), followed by quantification of fluorescence signals of individual telomeres using ImageJ or the TFL-Telo software (a gift from P. Lansdorp). Representative data from at least 30 metaphases of each genotype were pooled and scored using GraphPad Prism (GraphPad). The frequencies of individual telomeres were plotted against the telomere signal intensity using arbitrary units. The percentage of telomere signal-free ends and telomere fragility (a chromatid with ≥2 telomere signals) were counted from at least 30 metaphases of each genotype.

Telomere replication stress was determined by IF using RPA32 (pSer33) and TRF2 primary antibodies (44). For detecting telomere dysfunction-induced foci (TIF) formation, 53BP1 and TRF2 primary antibodies were used. The numbers of RPA32 (pSer33) foci or 53BP1 foci that colocalized with TRF2 per nucleus were scored. PLA utilizing TRF2 and 53BP1 as proximity ligation targets was also employed to determine TIFs (42).

DNA-RNA hybrid immunoprecipitation (DRIP)

Genomic DNA was sonicated using an ultrasonicator (Diagenode) with a water bath (settings: 30s 'on'/30s 'off'; power: 'high'; time: 5 min). 5 μg of nucleic acid was incubated with 1 μg of S9.6 antibody in IP buffer (1% Triton X-100, 0.1% SDS, 10 mM HEPES, pH 7.2, 275 mM NaCl, 0.1% sodium deoxycholate) for 6 h at 4°C on a rotating wheel. For RNase H1 control, nucleic acids were treated with 60 U of RNase H1 at 37°C for 3 h prior to incubation with the S9.6 antibody. The immunocomplexes were incubated with sheared E. coli DNA and BSA-blocked Protein A/G PLUS-Agarose beads (Santa Cruz Biotechnology, 10% v/v) for 2 h at 4°C on a rotating wheel. Beads were washed in IP buffer four times by centrifugation at 800 g and incubated in an elution solution (10 mM EDTA, 50 mM Tris–Cl, pH 8, 0.5% SDS) containing 40 μg/ml RNase A and 10 μg/ml proteinase K (Sigma-Aldrich) for 30 min at 50°C. Beads were subjected to centrifugation as described above, and the resulting supernatant was collected. Isopropanol was used to precipitate DNA in the supernatant. DNA samples were subjected to dot-blot analysis using the Telo-C-Biotin $(CCCTAA)_4$ probe (IDT DNA).

In vitro R-loop assembly and electrophoretic mobility shift assay (EMSA)

Construction of RNA:DNA hybrids

Oligonucleotides were generated and gel-purified (IDT DNA). Three-stranded RNA:DNA hybrid with the displaced single-stranded DNA were constructed according to previously established methods (45) with minor modifications, such as the use of TERRA and telomere repeat sequences. The oligonucleotides mimic the TERRA-like invading strand (INV, 5′-UUGAGAACUGGAUGGUG$(UUAGGG)_5$–3′), the telomere C-strand (TC, 5′-TCAA GCTCGGTCTGCAGTCAGGATGATT GT$(CCCTAA)_5$TCTGCACTCGAGACTCACGTCCTGGTCACG-3′) and its complemental strand (TG, 5′-CGTGACCAGGAC

GTGAGTCTCGAGTGCAGACCTTTTTTTTTTTTTTT TTTTTTTTTTTTACAATCATCCTGACTGCAGACCGA GCTTGA-3′) (46). TERRA-like invading strand hybridized with the melted regions of TC and TG duplex DNA to form an R-loop structure. Annealing reactions (20 μl) were conducted in 50 mM LiCl using a PC-100 Peltier thermal cycler (MJ Research). INV oligonucleotides were incubated with the complementary strand (TC) at 95°C for 5 min and cooled stepwise (1.2°C/min) to 60°C. TG was then added to the reaction and incubated at 60°C for 1 h, followed by cooling stepwise (1.2°C/min) to 25°C.

Emsa

Purified RBM14 and TRF2

GST-RBM14 and GST-TRF2 proteins were purchased (Novus Bio, H00010432-P01, MB291 and H00007014-P01, M8191, respectively).

TERRA binding with RBM14 or TRF2

Protein was diluted in a dilution buffer (25 mM Tris–HCl, pH 7.5, 10% (v/v) glycerol, 0.5 mM EDTA, 50 mM KCl, 1 mM DTT and 0.01% NP40). Increasing concentrations of RBM14 or TRF2 were incubated with TERRA $(\underline{UUAGGG})_5$ or the corresponding antisense $(CCCUAA)_5$ oligonucleotides at 37°C for 10 min in 20 μl of buffer (50 mM Tris–HCl, pH 7.5, 50 mM KCl, 1 mM $MgCl_2$, 1 mM ATP). The reaction mixtures were then crosslinked with 0.01% glutaraldehyde for 10 min. Products were resolved using 0.8% agarose gels supplemented with 10 mM KCl and stained with SYBR™ Safe DNA Gel Stain (ThermoFisher) at 4°C for 50 min (6.5 V cm^{-1}). Free RNA and RBM14-bound RNA were imaged using the ChemiDoc imager (Bio-Rad) and quantified with ImageQuant TL software (GE Healthcare Life Sciences) to determine the percentage of bound substrate [RNA bound/(RNA bound + RNA unbound)] in each gel. The data was displayed using GraphPad Prism software, with a one-site binding curve (hyperbola) fitted to the data. K_d values from three experiments were averaged and the standard deviation calculated. The one-site binding curve equation was utilized as $Y = (B_{max}*X)/(K_d + X)$, in which X is ligand concentration (nM), Y is binding (%), B_{max} is maximum binding (%) and K_d is the dissociation constant (nM).

R-loop formation assay with RBM14

The effect of RBM14 on the formation of R-loop structures was examined according to the published protocols with minor modifications (45). 30 μl of an oligonucleotide and protein mixture consisting of the INV oligonucleotides, varying amounts of purified RBM14 or TRF2, and 1× reaction buffer (50 mM Tris–HCl, pH 8.0, 5 mM $MgCl_2$, 0.5 mM $MnCl_2$, 40 mM NaCl, 1 mM DTT and 0.1 mg/ml BSA) were incubated at 37°C for 15 min. An aliquot of 20 μl was mixed with 8 μl of 3X native stop dye. Annealing reactions (20 μl) were conducted in 50 mM LiCl using a PC-100 Peltier thermal cycler. The TC oligonucleotides were incubated with the complementary strand (TG) at 95°C for 5 min and cooled stepwise (1.2°C/min) to 60°C. The oligonucleotide and protein mixtures were then added to the TC/TG mixture and incubated at 60°C for 1 h, followed by cooling stepwise (1.2°C/min) to 25°C. The mixture was analyzed on an 8% polyacrylamide native gel and visualized by staining with SYBR™ Safe DNA Gel Stain (ThermoFisher).

Statistical analysis

Statistical values are reported in the figure legends. The data are shown as the means ± standard deviations (SDs) from the indicated independent experiments. P values were calculated using the Student's *t*-test or one-way ANOVA. The latter was employed for comparing three or more groups.

Results

RBM14 is localized at telomeres in ALT human cancer cells

RBM14 was previously identified as a putative TERRA-binding protein in ALT cells by chromatin DNA–RNA hybrid immunoprecipitation (DRIP) analysis (30). To determine the presence of RBM14 at telomeres in U2OS ALT cells, we conducted chromatin immunoprecipitation (ChIP) utilizing antibodies that specifically target RBM14, the telomeric protein TRF1, or IgG. The DNA contents derived from ChIPs were evaluated by dot blotting employing probes that detect telomeric or genome-wide dispersed Alu repeats. Similar to TRF1, RBM14 immunoprecipitated telomeric DNA, but IgG did not show any binding affinity. RBM14 also immunoprecipitated Alu repeats, whereas TRF1 and IgG, as anticipated, did not exhibit any binding affinity (Figure 1A). These findings suggest that RBM14 is localized to telomeres in ALT cells.

It has been shown that RBM14 is recruited to I-Ppol- or microlaser-induced DNA damage sites in a PARP1- and KU-dependent manner (31). Notably, under normal physiological conditions, the immunoprecipitation of telomeric DNA by RBM14 showed comparable efficacy in U2OS cells that were treated with mock, a PARP1 inhibitor (Olaparib), or a KU inhibitor (STL127705) (Figure 1B). In contrast, a reduction of approximately 40% in telomeric DNA contents was observed in the RBM14 ChIP, when the levels of TERRA were depleted by approximately 50% in U2OS cells. TERRA depletion was achieved through transfection of TERRA antisense oligonucleotides with locked nucleic acid chemistry, along with a gapmer that facilitated TERRA degradation by RNase H (30) (Figure 1C and D). These findings suggest that under normal physiological conditions, PARP1 and KU play no role in the localization of RBM14 to telomeres; however, TERRA is required for RBM14 to effectively interact with telomeres in ALT cells.

To further validate the association between RBM14 and telomeres, we depleted RBM14 in U2OS cells using two distinct small interference RNAs ($siRBM14^{\#1}$ and $siRBM14^{\#2}$). RBM14 depletion was confirmed by western blot (Figure 1E) and immunofluorescence (IF)(Supplementary Figure S1A), in comparison to the control group treated with a non-targeting siRNA (siNT). Following the depletion of RBM14, a significant decrease of around 70% was observed in the amount of telomeric DNA in the RBM14 ChIP (Figure 1F). In addition, we showed that RBM14 co-localized with the telomeric protein TRF2 and TERRA by IF combined with TERRA RNA fluorescent *in situ* hybridization (TERRA RNA-FISH)(Supplementary Figure S1B) and with ALT-associated PML bodies by IF analysis (Supplementary Figure S1C). Furthermore, the proximity ligation assay (PLA) yielded positive signals when TRF2 and RBM14 were used as proximity lig-

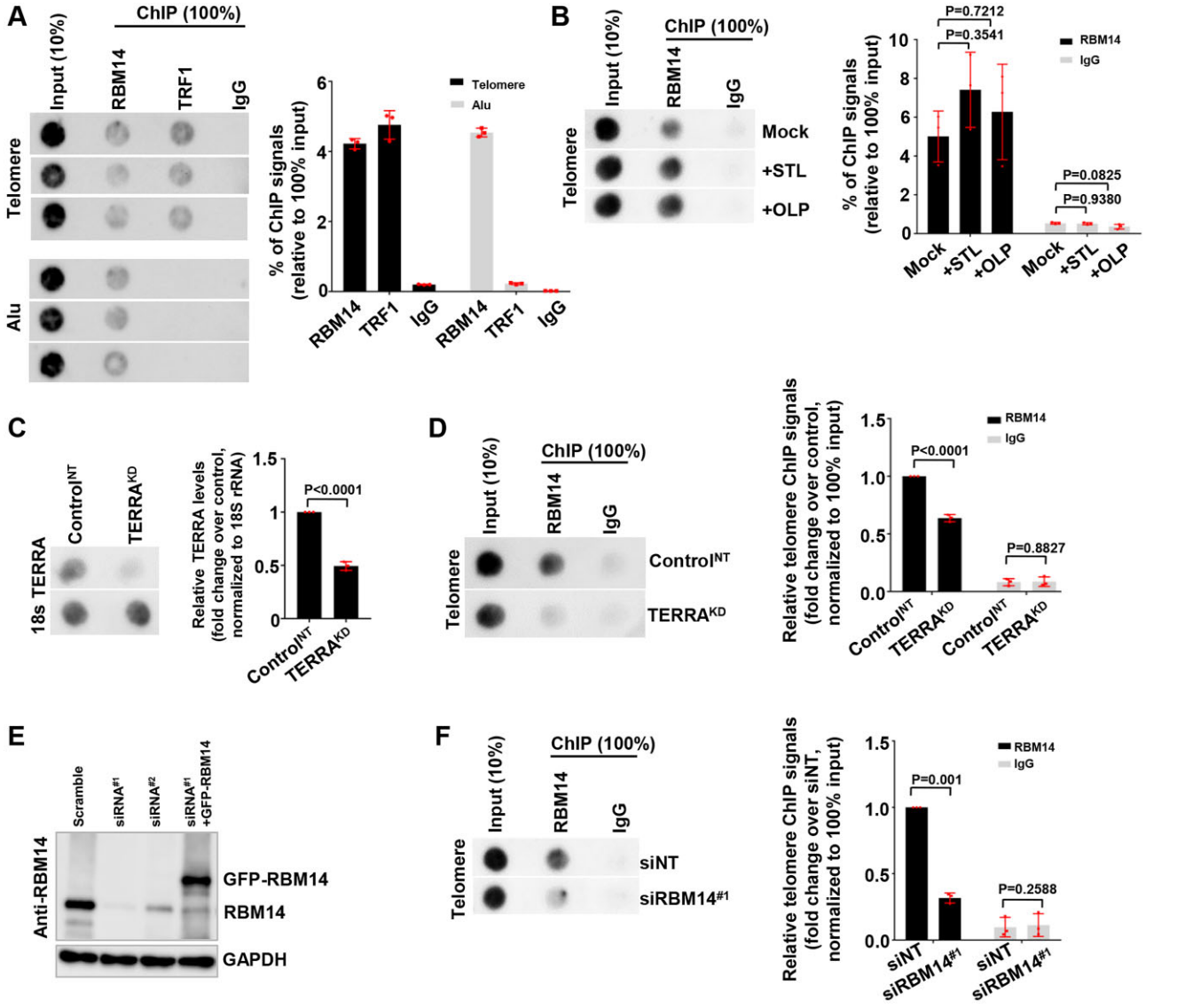

Figure 1. RBM14 is associated with telomeres in human ALT cells. (**A**) Dot blot analysis of telomere and Alu DNA contents in the indicated ChIP and input from U2OS cells using the Telo-C-Biotin $(CCCTAA)_4$ or Alu probes. TRF1 and IgG ChIP served as the positive and negative controls, respectively. The percentage of telomeric and Alu repeat signals in the indicated ChIPs relative to the signals corresponding to 100% input was shown as the mean ± SD of three independent experiments. (**B**) Dot blot analysis of telomere DNA contents in the indicated ChIP and input from U2OS cells treated with either 1 μM Olaparib (OLP) or 2 μM STL127705 (STL) for 24 h. IgG ChIP served as a negative control. The telomeric repeat signal was detected using the Telo-C-Biotin $(CCCTAA)_4$ probe. The percentage of telomeric repeat signals in the indicated ChIP relative to the signals corresponding to 100% input was shown as the mean ± SD of three independent experiments. (**C**) Dot blot analysis of TERRA and 18S contents in U2OS cells transfected with either non-targeting (NT) or TERRA antisense (TERRA KD) LNA gapmers using the Telo-C-Biotin $(CCCTAA)_4$ and 18S probes. The relative TERRA levels were normalized against the values for 18S and non-targeting controls and shown as the mean ± SD of technical triplicates. (**D**) Dot blot analysis of telomere DNA contents in the indicated ChIPs and input from U2OS cells transfected with either non-targeting or TERRA antisense LNA gapmers using the Telo-C-Biotin $(CCCTAA)_4$ probe. IgG ChIP served as the negative control. The relative telomeric repeat values in the indicated ChIPs were normalized against the values corresponding to 100% input and non-targeting control, which was set to a value of 1. The data were shown as the mean ± SD of three independent experiments. (**E**) Western blot analysis of RBM14 protein levels in U2OS cells transfected with non-targeting siRNA (siNT), RBM14 siRNA#1 ($siRBM14^{\#1}$), RBM14 siRNA#2 ($siRBM14^{\#2}$), or $siRBM14^{\#1}$ plus the plasmid expressing siRNA-resistant GFP-RBM14 for 72 h. GAPDH serves as the loading control. (**F**) Dot blot analysis of telomere DNA contents in the indicated ChIPs and input from U2OS cells transfected with either siNT or $siRBM14^{\#1}$ using the Telo-C-Biotin $(CCCTAA)_4$ probe. IgG ChIP served as a negative control. The mean ± SD of three independent experiments was used to represent the relative telomeric repeat values in the indicated ChIPs, normalized to the values corresponding to 100% input and siNT control (set to a value of 1).

ation targets. The specificity of PLA in detecting telomeric RBM14 was verified by the colocalization of PLA signals with TRF2 and RBM14 IF signals (Supplementary Figure S1D). Collectively, our findings support the notion that RBM14 is localized to telomeres in ALT cells.

RBM14 interacts with TERRA *in vivo* and *in vitro*

Next, we validated the interactions between RBM14 and TERRA in U2OS cells. RNA immunoprecipitation (RIP) was carried out utilizing the RBM14, TRF2, or IgG antibodies, with or without RNase A treatment. Following dot blotting, the Telo-C-Biotin $(CCCTAA)_4$ probe was used to identify TERRA. In line with a previous report (29), we found that TRF2 immunoprecipitated TERRA, which served as a positive control (Figure 2A). Similarly, RBM14 immunoprecipitated TERRA, but TERRA was almost undetectable in both the anti-IgG RIP and the anti-RBM14 RIP that was treated with RNase A (Figure 2A). The levels of TERRA in the anti-RBM14 RIP decreased by approximately 50% after RBM14 depletion (Figure 2B, upper panel). In contract, the TERRA sense $(GGGATT)_4$ probe detected non-specific signals in both anti-IgG RIP and anti-RBM14 RIP of cells transfected with either non-targeting or RBM14 siRNAs (Figure 2B, lower panel). These results revealed a specific interaction between RBM14 and TERRA *in vivo*.

To determine the direct binding of RBM14 to TERRA, we performed an *in vitro* electrophoretic mobility shift assay (EMSA). TERRA $(UUAGGG)_5$ or the corresponding anti-sense $(CCCUAA)_5$ oligonucleotides were incubated with increasing concentrations of purified RBM14 (Figure 2C). There was a dose-dependent increase in the binding of TERRA and anti-sense oligonucleotides to RBM14, with a twofold preference for TERRA (Figure 2D and E). In addition, the amount of TERRA oligonucleotides bound to TRF2 rose as the amount of purified TRF2 increased (Supplementary Figure S2), corroborating earlier findings (27–29,47). Collectively, our observations are consistent with the idea that RBM14, similar to TRF2, directly binds to TERRA *in vitro*.

RBM14 modulates TERRA levels in ALT cells

To determine if RBM14 regulates TERRA *in vivo*, the total levels of TERRA were determined in U2OS cells that were transfected with either siNT or siRBM14, or co-transfected with siRBM14 and RNAi-resistant GFP-RBM14 by northern blot and RNA dot blot using the Telo-C-Biotin $(CCCTAA)_4$ probe. Northern blot analysis revealed a 1.2-fold increase in TERRA expression following the depletion of RBM14 (Figure 3A). RNA dot blot analysis yielded comparable results, showing an approximately twofold increase in TERRA expression in RBM14 knockdown cells (Figure 3B). In contrast, TERRA levels in RBM14 knockdown cells expressing GFP-RBM14 (Figure 1E) were comparable to those in siNT-transfected control cells (Figure 3A and B). After RNase A treatment, neither Northern blot nor RNA dot blot detected any TERRA signals (Figure 3A and B). TERRA RNA-FISH was also employed to determine the expression of TERRA in U2OS cells. RBM14 knockdown cells displayed an increased number of TERRA signals than siNT-transfected control cells, with an average of 7 and 13 foci per siNT- and siRBM14-transfected cell, respectively. Conversely, the ectopic expression of GFP-RBM14 resulted in a significant reduction of TERRA signals in RBM14 knockdown cells, with an average of 3 foci per cell (Figure 3C and Supplementary Table S3).

Next, we assessed chromosome-end-specific TERRA by RT-qPCR in U2OS cells (Figure 3D). Among the chromosome-end-specific TERRA we tested, chromosome 7p exhibited the most pronounced levels of TERRA, whereas the levels of TERRA on the remaining chromosome ends were relatively low. Following the depletion of RBM14, TERRA exhibited variable degrees of increase relative to the 7p siNT control, with a 7.6-fold increase in 7p and moderate increases at other chromosomal ends. Conversely, the ectopic expression of GFP-RBM14 resulted in a reduction of TERRA transcripts in RBM14 knockdown cells to a level similar to that of the siNT control. Collectively, our findings indicate that RBM14 functions as a suppressor of TERRA in ALT cells.

RBM14 adversely affects TERRA stability and transcription in ALT cells

The levels of TERRA could be influenced by its stability and/or transcription *in vivo*. We first investigated the stability of TERRA in U2OS cells that were transfected with either siNT or siRBM14, or co-transfected with siRBM14 and RNAi-resistant GFP-RBM14. RT-qPCR assay was conducted to analyze the levels of chromosome end-specific TERRA at multiple time intervals after cells were treated with 7.5 nM actinomycin D, a gene transcription inhibitor (Figure 4A and Supplementary Table S3). Following the depletion of RBM14, the half-life of TERRA, measured at 6 h, increased by 3.44-fold, 1.48-fold and 1.81-fold at 7p, 16p and 20q, respectively. In contrast, the degradation of TERRA, observed at 12 h, decreased by 2.82-fold, 2.51-fold, 2.58-fold and 1.42-fold at 7p, 10q, 13q and 16p, respectively. The ectopic expression of GFP-RBM14 resulted in the restoration of TERRA half-life or degradation in RBM14 knockdown cells to a level similar to that observed in the siNT control cells. The RNA dot blot analysis also revealed comparable patterns in the total levels of TERRA in U2OS cells following the treatment with 7.5 nM actinomycin D (Figure 4B and C). These results indicate that RBM14 depletion boosted TERRA stability.

RBM14 functions at the interface of transcriptional coactivation (34). To investigate the involvement of RBM14 in the regulation of TERRA transcription, we examined U2OS cells that were transfected with either siNT or siRBM14. ChIP-qPCR was employed to ascertain the association between RBM14 and subtelomeric regions that have been previously implicated in TERRA transcription (48)(Figure 5A). RBM14 was detected at the subtelomeres of 10q and 13q, whereas the association between RBM14 and these loci decreased upon RBM14 depletion, with 4.72-, 3.65- and 3.18-fold changes at the 396, 1122 and 1997 bp positions on 10q, and 3.57-, 1.85- and 2.39-fold changes at the 152, 957 and 6545 bp positions on 13q, respectively (Figure 5B and Supplementary Table S3).

As the expression of TERRA is influenced by RNAPII occupancy and chromatin organization at these subtelomeric loci (48), we determined the binding of RNAPII and the patterns of histone modifications in U2OS cells that were transfected with either siNT or siRBM14. In comparison to the siNT control, RBM14 depletion increased the occupancy of RNAPII at the 10q and 13q loci, with 1.13-fold change at the 396 bp position and 1.23-fold change at the 1997 bp position on 10q, and a 1.39-fold change at the 152 bp position on 13q (Figure 5C and Supplementary Table S3). In addition,

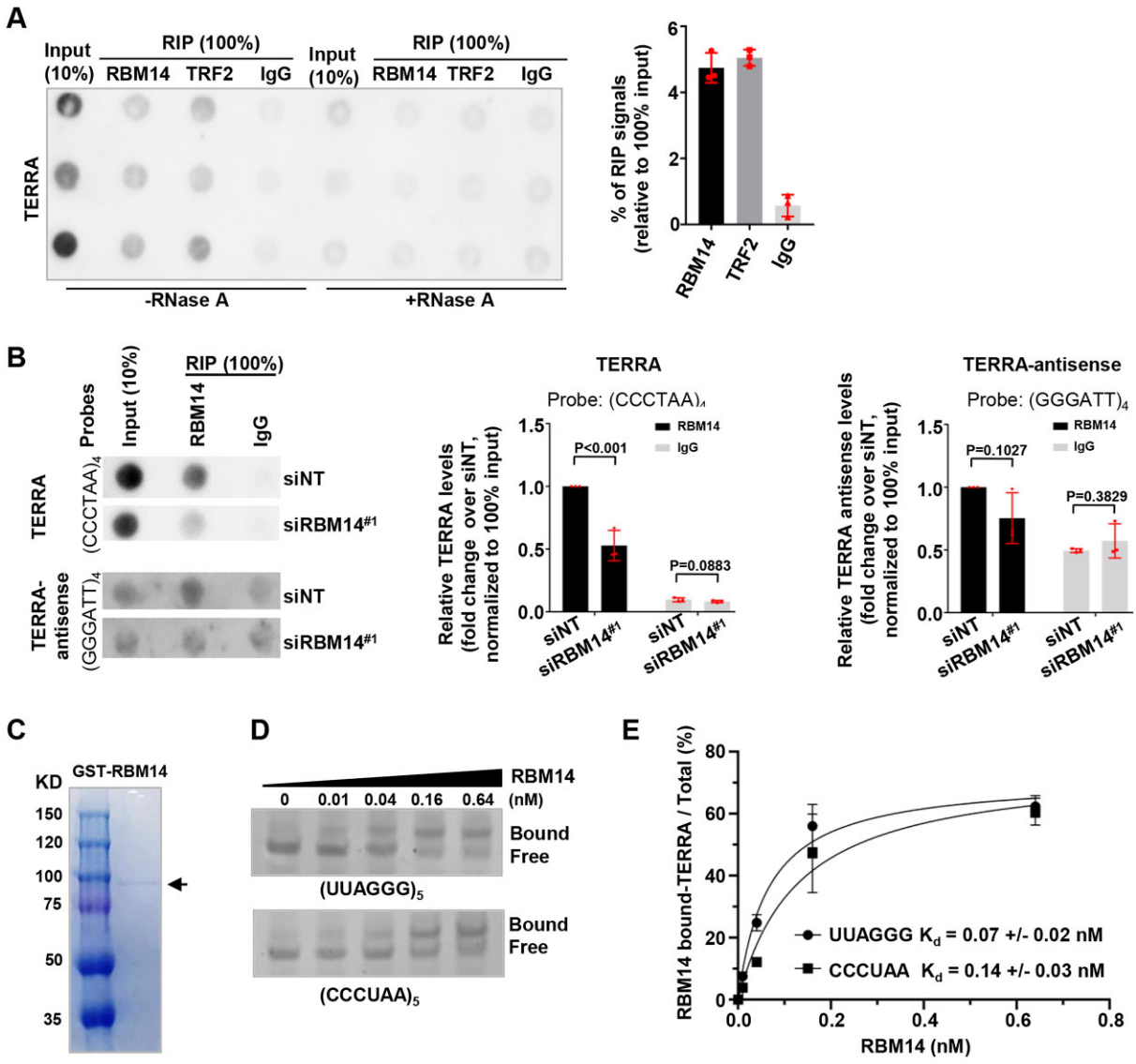

Figure 2. RBM14 is associated with TERRA *in vivo* and in *vitro*. (**A**) Dot blot analysis of TERRA contents in native RNA immunoprecipitation of RBM14, TRF2 and IgG in U2OS cells using the Telo-C-Biotin $(CCCTAA)_4$ probe. IgG and RNase A treatments served as the negative controls, whereas TRF2 was a positive control. The mean ± SD of three independent experiments was used to represent the percentage of TERRA signals in the indicated RIPs relative to the values corresponding to 100% input. (**B**) Dot blot analysis of TERRA or TERRA antisense levels in native RNA immunoprecipitation of RBM14 and IgG in U2OS cells transfected with either siNT or siRBM14$^{\#1}$ using either $(CCCTAA)_4$ or $(GGGATT)_4$ probes labeled with biotin. IgG served as a negative control. The relative TERRA or TERRA antisense values were normalized to the value corresponding to 100% input and siNT control (set to 1). The data were shown as the mean ± SD of three independent experiments. (**C**) Coomassie blue staining of purified GST-RBM14 proteins (0.4 μg) resolved on an SDS-polyacrylamide gel. (**D, E**) EMSA analysis of RBM14's affinity for TERRA and the corresponding anti-sense RNA oligonucleotides. RNA substrates (0.01 nM) were incubated with increasing concentrations of purified RBM14 protein. Free and RBM14-bound substrates are as indicated. The percentage of RNA substrates bound to RBM14 at each RBM14 concentration was normalized to the total and shown as the average ± SD of three independent experiments. The average K_d values were obtained from three experiments, and the standard deviation was determined.

we monitored H3K4me3 and H3K9me3 at these chromosome loci, which have been linked, respectively, to increased or decreased transcription elongation. RBM14 depletion led to an increase in H3K4me3 occupancy at the 10q and 13q loci. The occupancy at the 396, 1122 and 1997 bp positions in the 10q region showed fold changes of 2.02, 1.82 and 1.84, respectively. Similarly, the occupancy at positions 152, 957 and 6545 bp in the 13q region exhibited fold changes of 2.23, 2.02 and 2.01, respectively. Conversely, RBM14 depletion diminished H3K9me3 occupancy in the 10q and 13q regions. In the 10q region, fold changes of 1.74, 1.72 and 1.73 were observed at positions 396, 1122 and 1997 bp, respectively. Similarly, fold changes of 1.36 and 1.45 were observed at positions 152 and 957 bp, respectively, in the 13q region (Figure 5D and E and Supplementary Table S3). These findings indicate that RBM14 modulates the levels of TERRA, possibly by regulating the stability and/or transcription of TERRA.

RBM14 inhibits the formation of R-loops at telomeres in ALT cells

RBM14 has been shown to associate with genomic R-loops in human cells (35). We therefore investigated the potential interaction between RBM14 and R-loops in U2OS cells using ChIP analysis with the RBM14 antibody, followed by reChIP

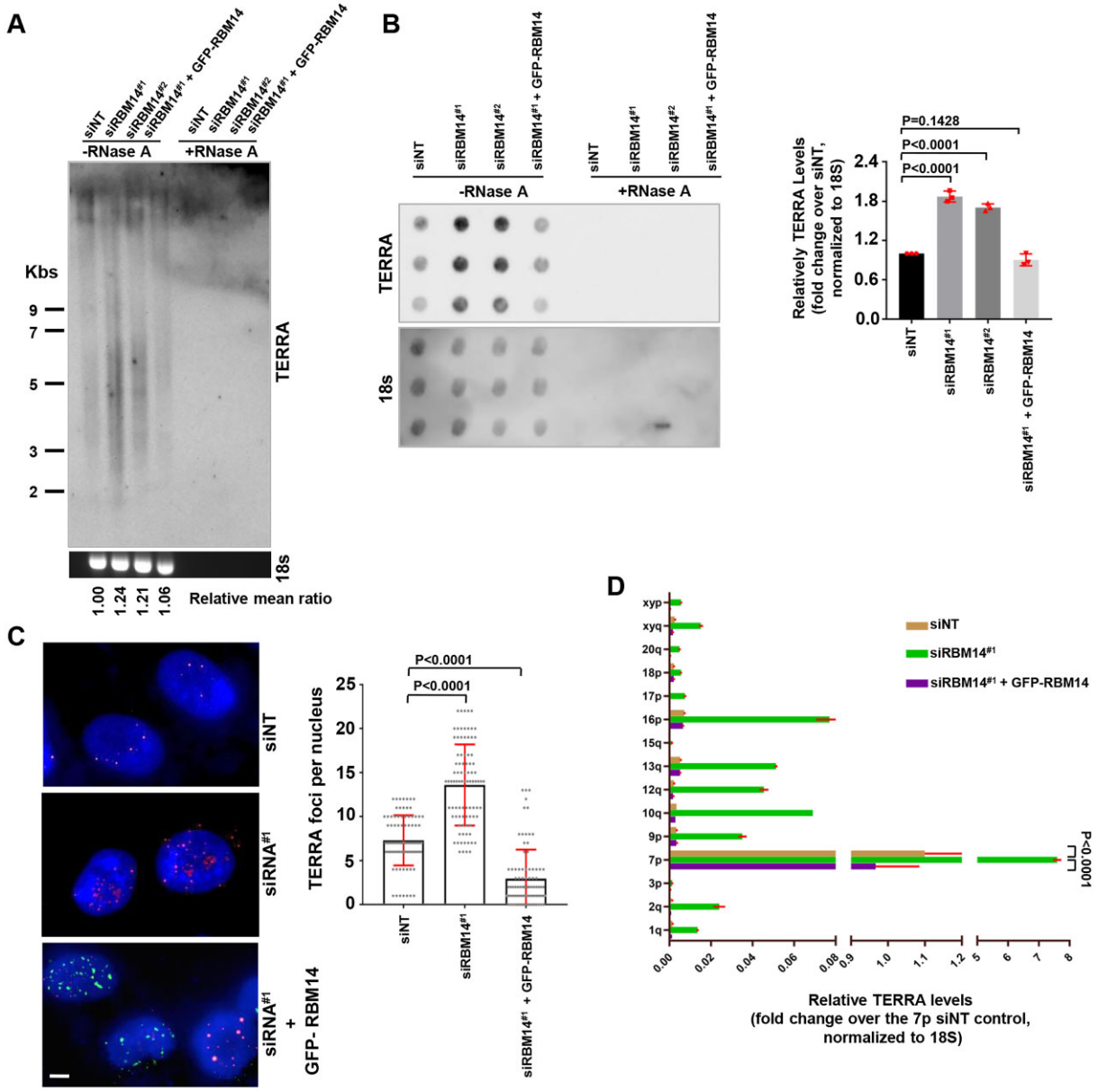

Figure 3. Depletion of RBM14 enhances TERRA levels in ALT cells. (**A**) Northern blot analysis of total TERRA in U2OS cells transfected with siNT, siRBM14$^{\#1}$, siRBM14$^{\#2}$ or siRBM14$^{\#1}$ plus GFP-RBM14 using the Telo-C-Biotin $(CCCTAA)_4$ probe. 18S stained with SYBR^{TM} Safe DNA Gel Stain served as a loading control. RNase A treatment served as a negative control. The mean TERRA signals were normalized against the signals for 18S and siNT (set to 1). (**B**) RNA dot blot analysis of total TERRA in the indicated U2OS cells using the Telo-C-Biotin $(CCCTAA)_4$ or 18S probes. RNase A treatment served as a negative control. The relative TERRA levels were normalized against the values for 18S and siNT (set to 1). The data were shown as the mean ± SD of three independent experiments. (**C**) RNA-FISH analysis of TERRA foci in the indicated U2OS cells using a Cy3-labeled Telo-C-PNA $(CCCTAA)_3$ probe. TERRA (red), GFP-RBM14 (green) and DAPI (blue) signals are shown. The quantification of TERRA foci per nucleus is presented. A total of 90, 88 and 87 cells were counted in siNT, siRBM14$^{\#1}$ and siRBM14$^{\#1}$ plus GFP-RBM14 groups, respectively. The data were shown as the mean ± SDs. Scale bars: 5 microns. (**D**) RT-qPCR analysis of chromosome end TERRA from the indicated U2OS cells. The TERRA values were normalized to the values corresponding to the 18S control. To display the variable nature of TERRA levels across chromosome ends, each chromosome end-specific TERRA was further normalized to the 7p siNT control (set to 1). The data were shown as the mean ± SDs of three independent experiments.

utilizing the S9.6 antibody, which recognizes R-loops (38,49). Telomeric R-loops derived from ChIP-reChIP were quantified using telomere qPCR. Both RBM14 and TRF2 were found to immunoprecipitate telomeric R-loop signals, with TRF2 serving as a positive control (Figure 6A), whereas RBM14 depletion resulted in a nearly 90% reduction in telomeric R-loop signals, serving as a negative control (Figure 6B). These results indicate that RBM14 interacts with telomeric R-loops in ALT cells. We could not rule out the possibility that RBM14 interacts with other types of RNA:DNA hybrids that may exist in telomeres and could be detected by the S9.6 antibody.

Increased TERRA levels, as a result of RBM14 depletion, may influence the formation of R-loops at telomeres. We utilized chromatin DNA-RNA hybrid immunoprecipitation (DRIP) with the S9.6 antibody (49,50) to assess the effect of RBM14 on telomeric R-loops in U2OS cells. Telomeric R-loops were extracted from the S9.6 pulldown and detected

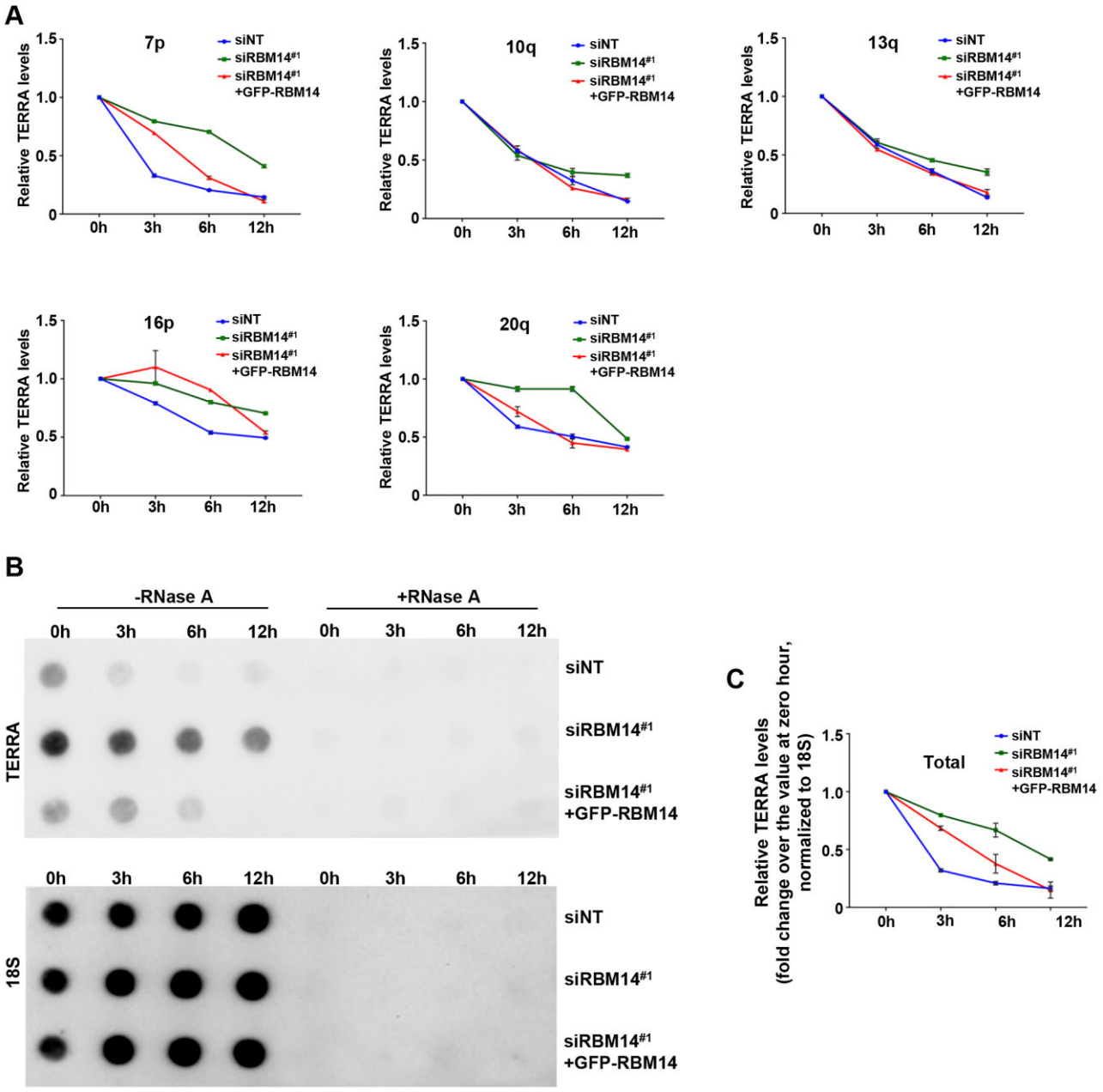

Figure 4. RBM14 knockdown leads to increased TERRA stability in ALT cells. (**A**) RT-qPCR of chromosome end TERRA from 7p, 10q, 13q, 16p and 20q in U2OS cells transfected with siNT, siRBM14$^{\#1}$ or siRBM14$^{\#1}$ plus GFP-RBM14. Cells were treated with 7.5 nM actinomycin D. (**B**, **C**) Dot blot analysis of total TERRA in the indicated U2OS cells treated with 7.5 nM actinomycin D using the Telo-C-Biotin $(CCCTAA)_4$ or 18S probes. The relative TERRA levels at each time point were normalized to the values of 18S and the zero hour (0 h) (set to 1). The data were shown as the mean ± SD of three independent experiments.

by the Telo-C-Biotin $(CCCTAA)_4$ probe after dot blotting. S9.6, but not IgG, pulled down telomeric R-loops, which were largely eliminated by RNase H1 treatment. The amount of telomere R-loops was further determined in U2OS cells transfected with either siNT or siRBM14. Compared to the siNT control cells, the quantity of telomeric R-loops increased 1.78-fold and 1.62-fold in siRBM14$^{\#1}$ and siRBM14$^{\#2}$ transfected cells, respectively (Figure 6C and Supplementary Table S3).

To substantiate our observations, we utilized IF analysis with the S9.6 and TRF2 antibodies (Figure 6D and E and Supplementary Table S3). In comparison to the siNT control cells, RBM14 knockdown cells exhibited an increase in S9.6 foci (11 and 28 events per siNT- and siRBM14 -transfected cell, respectively). A portion of these foci were found to colocalize with TRF2 signals (3 and 6 events per siNT- and siRBM14-transfected cell, respectively). The colocalization of S9.6 and TRF2 signals was significantly reduced in RBM14 knockdown cells with ectopic expression of GFP-RBM14 or GFP-RNase H1 (1.7 and 0.8 foci per GFP-RBM14- and GFP-RNase H1-positive cell, respectively). Our findings indicate that RBM14 exerts an inhibitory effect on the formation of RNA:DNA hybrids, such as R-loops in ALT telomeres.

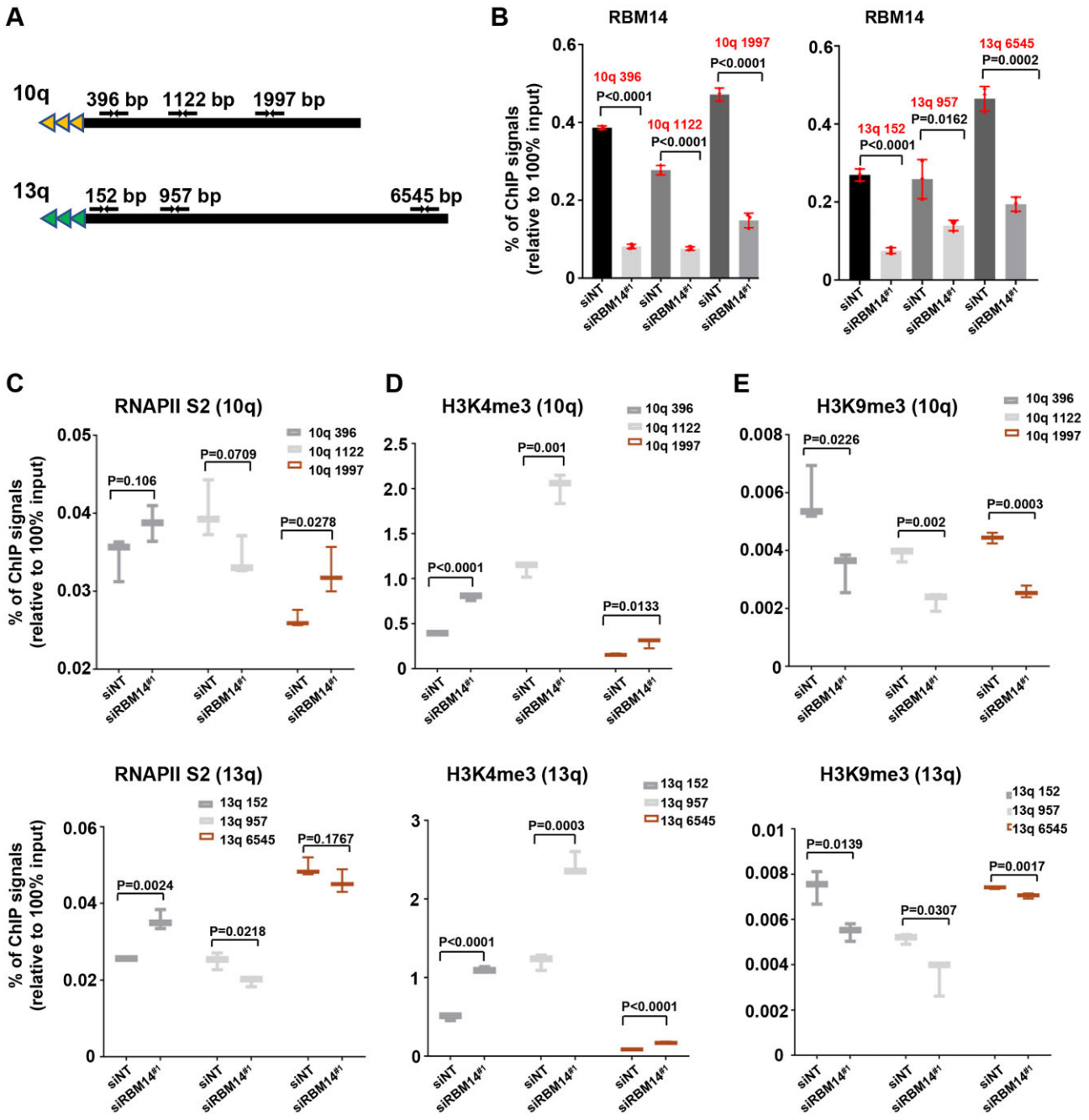

Figure 5. The effect of RBM14 depletion on RNAPII binding and chromatin architecture of RBM14 elements at the 10q and 13q subtelomeric loci in ALT cells. (**A**) A schematic diagram illustrating the spatial arrangement of PCR primers that encompass the 10q and 13q subtelomeric loci. (B–E) ChIP-qPCR analysis of RBM14 (**B**), RNAPII serine 2 (S2) phosphorylation (**C**), histone H3 K4 (**D**) and histone H3 K9 tri-methylation (**E**) at 10q and 13q in U2OS cells transfected with either siNT or siRBM14$^{\#1}$. The percentage of ChIP values relative to the value corresponding to 100% input was shown as the mean ± SD of three independent experiments.

RBM14 inhibits TERRA from forming R-loops *in vitro*

Since telomere R-loop formation involves TERRA (20,21), we examined whether RBM14 regulates TERRA to form R-loops by EMSA. In order to generate a three-stranded R-loop-like RNA:DNA structure, we utilized a TERRA-like RNA oligonucleotide (INV) together with two DNA oligonucleotides, TC and TG. The TC oligonucleotide contains telomere repeats located in the middle region, while the TG oligonucleotide serves as the complimentary strand with non-complementary sequences located opposite the telomere repeats in TC (Figure 7A). Figure 7B exhibited the native gel electrophoresis, displaying the positions of a mix containing INV, TC and TG (lanes 1–7), a mix containing TC and TG (lane 8) and each individual oligonucleotide (lanes 9–11). *In vitro* INV formed a complex with TC and TG (lane 7), which mimicked the three-stranded R-loop structure. INV was incubated with increasing concentrations of purified RBM14, prior to the addition of TC and TG to the reaction mixture (lanes 2–6). When RBM14 concentrations increased, R-loops decreased (Figure 7B, lanes 2–6; and Figure 7C). RNase H1 has been documented to disassemble

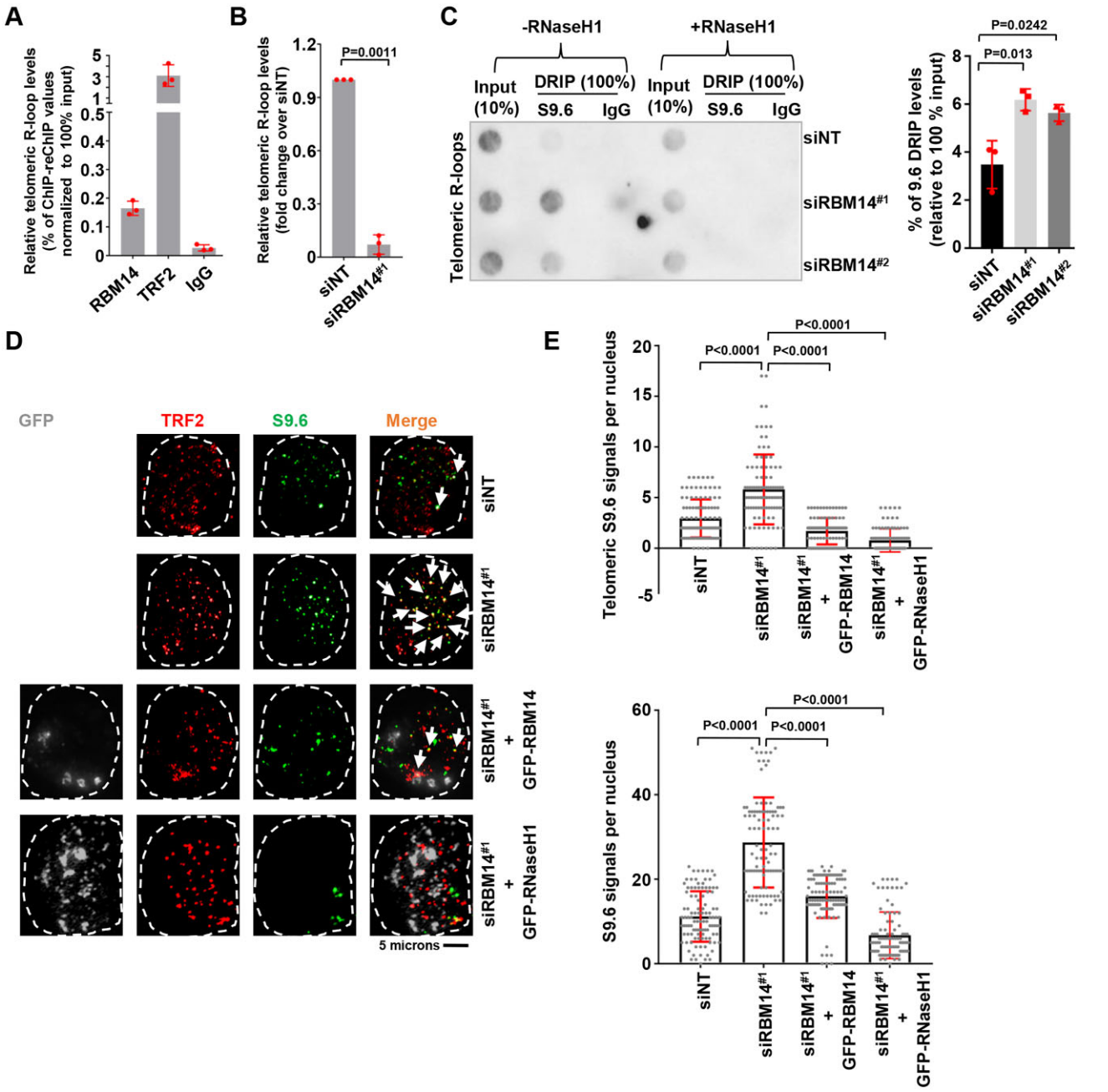

Figure 6. RBM14 deficiency increases R-loops at telomeres in ALT cells. (**A**) Telomeric R-loop levels in RBM14, TRF2 or IgG ChIP and S9.6 reChIP assays in U2OS cells by telomere qPCR analysis. TRF2 and IgG served as the positive and negative controls, respectively. The percentage of ChIP-reChIP values relative to the values corresponding to 100% input was shown as the mean ± SD of three independent experiments. (**B**) Telomeric R-loop levels in RBM14 ChIP and S9.6 reChIP in U2OS cells transfected with either siNT or siRBM14$^{\#1}$ by telomere qPCR analysis. The relative telomeric R-loop values in the indicated ChIP-reChIP were normalized to the value corresponding to the siNT control (set to 1). (**C**) Dot-blot analysis of R-loops at telomeres in U2OS cells transfected with either siNT or siRBM14$^{\#1}$ using the Telo-C-Biotin $(CCCTAA)_4$ probe. DRIP was used to isolate R-loops in cells employing the S9.6 antibody. RNase H1 treatment served as a negative control. The percentage of DRIP signals relative to the values corresponding to 100% input was shown as ± SDs from three independent experiments. (**D**, **E**) Immunofluorescence analysis of R-loops at telomeres in U2OS cells transfected with siNT, siRBM14$^{\#1}$, siRBM14$^{\#1}$ plus GFP-RBM14 (grey), or siRBM14$^{\#1}$ plus GFP-RNaseH1 (grey). Telomeric R-loops were identified by colocalization of S9.6 (green) and TRF2 (red) signals. GFP-RNase H1 served as a control. The numbers of telomeric and genomic S9.6 signals per nucleus in the indicated U2OS cells are shown. To quantify telomeric S9.6 foci, a total of 107, 98, 106 and 100 cells were evaluated in siNT, siRBM14$^{\#1}$, siRBM14$^{\#1}$ plus GFP-RBM14, and siRBM14$^{\#1}$ plus GFP-RNase H1 groups, respectively. To quantify genomic 9.6 foci, a total of 96, 99, 98 and 94 cells were evaluated in siNT, siRBM14$^{\#1}$, siRBM14$^{\#1}$ plus GFP-RBM14, and siRBM14$^{\#1}$ plus GFP-RNase H1 groups, respectively. Scale bar: 5 microns.

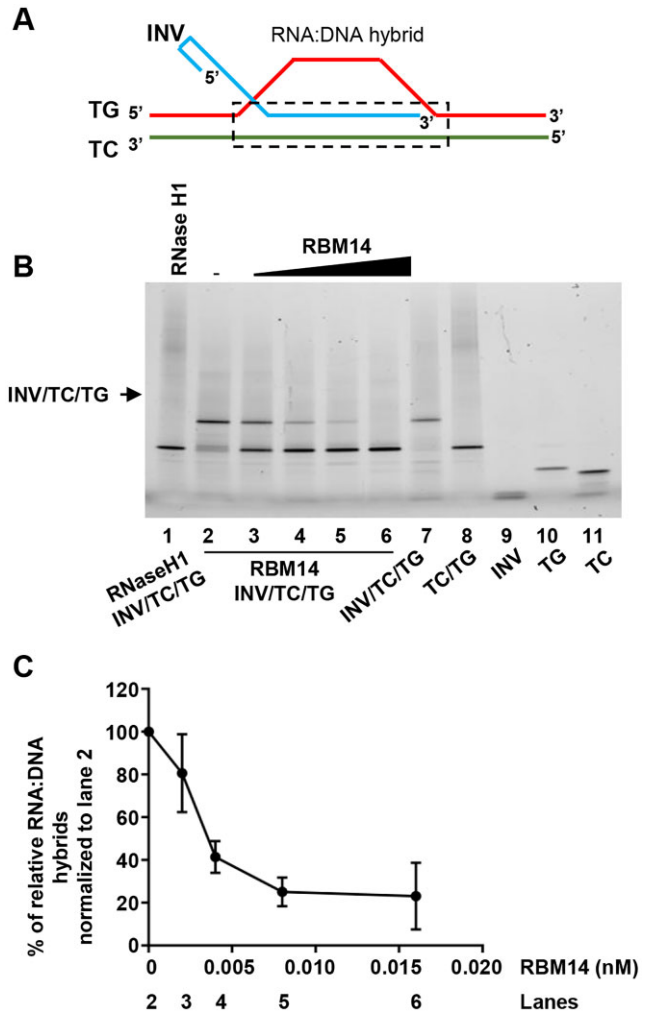

Figure 7. RBM14 inhibits TERRA from forming an RNA:DNA hybrid *in vitro*. (**A**) Assembly of a three-stranded RNA:DNA hybrid configuration using INV, TG and TC oligonucleotides. INV stands for TERRA-like RNA oligonucleotides. TC contains telomere repeats in its central region, and TG is the complementary DNA strand with non-complementary oligonucleotides positioned in opposition to the telomere repeats present in the TC sequence. (**B**) Native gel electrophoresis of INV, TG and TC oligonucleotides in combination (lanes 1–8) as well as individually (lanes 9–11). INV (0.0005 nM) was incubated with increasing amounts of purified RBM14 (0, 0.002, 0.004, 0.008 and 0.016 nM), and then with TC (0.0015 nM) and TG (0.0015 nM) substrates (lanes 2–6). With increasing RBM14 protein concentrations, the INV/TC/TG complex decreased. RNase H1 served as a control for R-loop resolution (Lane 1). (**C**) The quantification of the INV/TC/TG complex (lanes 2–6) in (B). The values were normalized to the value corresponding to lane 2 (set to 100%). The data are shown as the mean ± SDs from three independent experiments.

R-loops by degrading TERRA within R-loops (20). As expected, the addition of RNase H1 to the reaction prevented the formation of R-loops (Figure 7B, lane 1). Our findings suggest that the interaction between RBM14 and TERRA may hinder the incorporation of TERRA into R-loops at telomeres.

Consistent with earlier findings that TRF2 promotes R-loop formation at telomeres (27,28), we found that the TERRA-like INV oligos in the R-loop configuration increased as TRF2 concentration rose (Supplementary Figure S3). Hence, it is plausible that RBM14 exerts inhibitory effects on the generation of telomeric R-loops facilitated by TERRA, whereas TRF2 could potentially counteract this effect.

RBM14 protects telomere integrity in ALT cells

Unscheduled accumulation of TERRA at telomeres correlates with the activation of the DNA damage response (DDR) (51). In addition, excessive R-loops at telomeres may impede the progression of the telomeric replication fork (21,52), hence triggering telomere dysfunction-induced DDR and DNA damage foci (TIF) formation (53,54). We determined TIFs in U2OS cells transfected with either siNT or siRBM14 by assessing the colocalization of the DNA damage response protein, p53 binding protein 1 (53BP1) and the telomeric protein TRF2 using IF analysis (54) (Figure 8A and Supplementary Table S3). RBM14 depletion resulted in an increase in the formation of TIFs, with an average of 2.81 and 4.52 TIF foci per siNT- and siRBM14- transfected cell, respectively. Conversely, the expression of GFP-RBM14 or RNase H1 resulted in a notable reduction in TIFs in RBM14 knockdown cells, with an average of 0.59 and 1.00 TIF foci per TIF foci per GFP-RBM14-positive and RNase H1-positive cells, respectively. Elevated TIFs were also confirmed in RBM14 knockdown cells by the PLA assay, wherein 53BP1 and TRF2 were employed as proximity ligation targets (42) (Supplementary Figure S4).

In order to provide additional evidence supporting the association between replication stress and the formation of TIFs following the depletion of RBM14, U2OS cells that were transfected with either siNT or siRBM14 were subjected to the treatment with low doses of the DNA polymerase inhibitor aphidicolin and analyzed for TIFs by IF analysis (Supplementary Figure S5 and Supplementary Table S3). Indeed, a treatment of 0.2 mM aphidicolin significantly increased the number of TIF foci in the RBM14 knockdown cells, compared to the siNT control cells, with an average of 2.01 and 4.58 foci per siNT- and siRBM14 -transfected cell, and 2.99 and 7.64 foci per aphidicolin-treated siNT- and siRBM14 -transfected cell, respectively. Notably, RBM14 knockdown also increased 53BP1 genome foci formation, with an average of 5.72 and 13.66 53BP1 foci per siNT- and siRBM14-transfected cell, respectively, and 0.2 mM aphidicolin treatment resulted in a further increase in the number of 53BP1 genome foci in the RBM14 knockdown cells compared to the siNT control cells, with an average of 8.71 and 25.87 foci per siNT- and siRBM14-transfected cell, respectively.

Elevated telomere replication stress can lead to the accumulation of the single-stranded DNA-binding protein RPA32 (phosphorylated at serine 33) at telomeres (44). IF analysis was therefore employed to assess the levels of RPA32 (pSer33) at telomeres in U2OS cells transfected with either siNT or siRBM14 (Figure 8B and Supplementary Table S3). RBM14 depletion increased the colocalization between RPA32 (pSer33) and TRF2 signals, with an average of 1.19 and 4.40 telomeric RPA32 foci per siNT- and siRBM14-transfected cell, respectively, whereas ectopic expression of GFP-RBM14 or RNase H1 in the RBM14 knockdown cells significantly reduced telomeric RPA32 pSer33 foci, to a level similar to that of the siNT control, with an average of 1.23 and 1.56 foci per GFP-RBM14 and RNase H1-positive cells, respectively. Overall, our findings indicate that RBM14 deficiency leads to the disruption of telomere replication and telomere integrity in ALT cells.

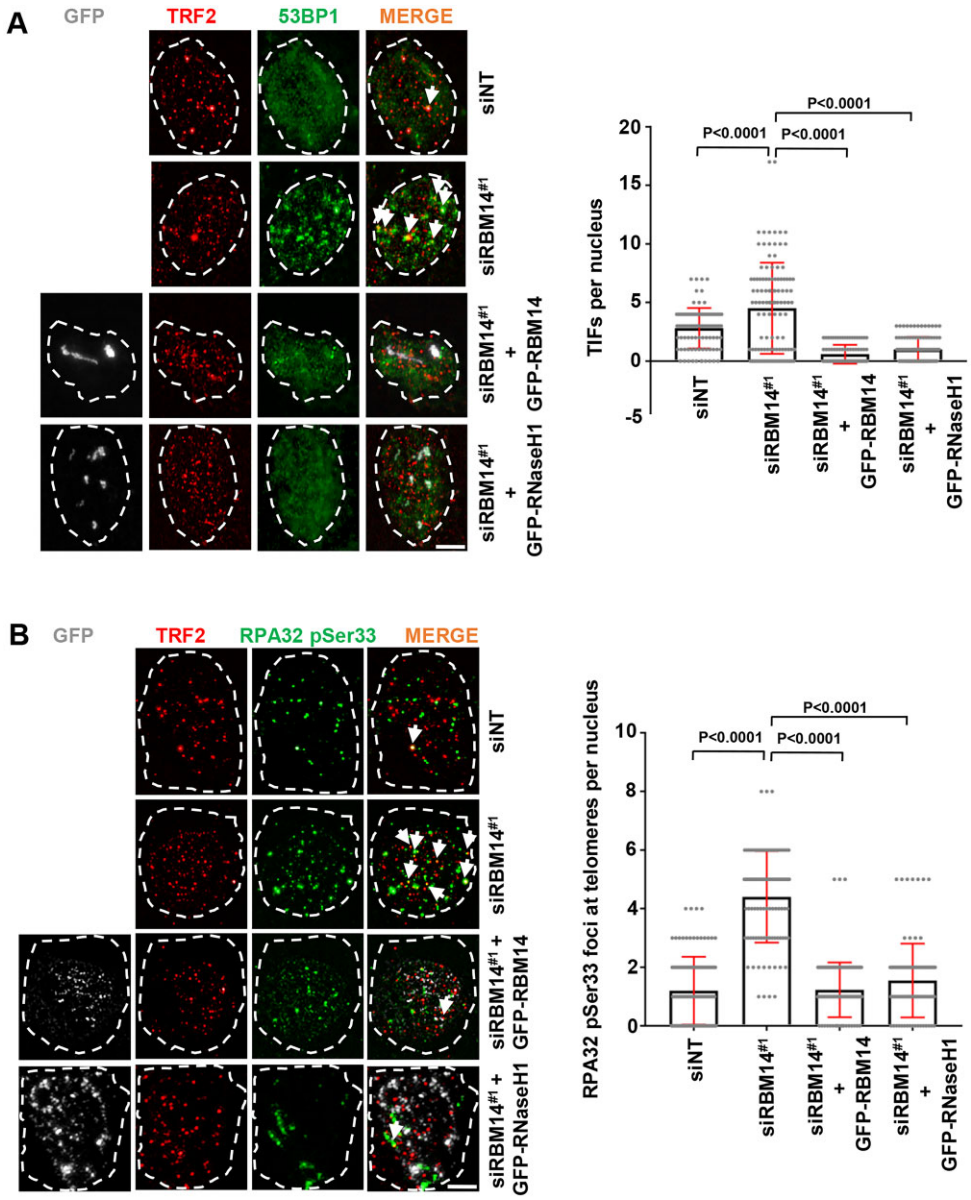

Figure 8. RBM14 suppresses telomeric DNA damage in ALT cells. (**A**) IF analysis of TIFs in U2OS cells transfected with siNT, siRBM14$^{\#1}$, siRBM14$^{\#1}$ plus GFP-RBM14 (grey) or siRBM14$^{\#1}$ plus GFP-RNaseH1 (grey). The colocalization of 53BP1 (green) and TRF2 (red) signals defined TIFs (arrows). The number of TIF signals per nucleus in the indicated U2OS cells is shown. A total of 98, 113, 93 and 95 cells were evaluated in siNT, siRBM14$^{\#1}$, siRBM14$^{\#1}$ plus GFP-RBM14 and siRBM14$^{\#1}$ plus GFP-RNase H1 groups, respectively. Scale bar: 5 microns. (**B**) IF analysis of telomeric pSer33 signals in the indicated U2OS cells. The colocalization of RPA32 pSer33 (green) and TRF2 (red) signals was scored (arrows). The number of telomeric pSer33 foci in each nucleus is shown in the indicated U2OS cells. A total of 114, 96, 104 and 94 cells were evaluated in siNT, siRBM14$^{\#1}$, siRBM14$^{\#1}$ plus GFP-RBM14, and siRBM14$^{\#1}$ plus GFP-RNase H1 groups, respectively. Scale bar: 5 microns.

RBM14 contributes to telomere length maintenance in ALT cells

RBM14 depletion results in increased TIF formation, especially after replication stress in U2OS cells. Excessive telomere DNA damage may exceed the capacity of HR-mediated repair, resulting in telomere loss and telomere fragility. Thus, we determined telomere length in U2OS cells transfected with either siNT or siRBM14 by quantitative telomere-FISH (Q-FISH) on metaphase spreads and southern blot-based telomere restriction fragment analysis. Q-FISH revealed that RBM14 knockdown resulted in an approximate 30% reduction in overall telomere signal intensity, with an average of 185, 125 and 139 arbitrary units in siNT-, siRBM14$^{\#1}$- and siRBM14$^{\#2}$-transfected cells, respectively (Figure 9A and B and Supplementary Table S3). RBM14 knockdown also led to a two-fold increase in the frequency of telomere-free chromosomal ends (TFEs), with an average of 14.87, 24.55 and 32.75 TFEs per siNT-, siRBM14$^{\#1}$- and siRBM14$^{\#2}$- transfected cell, respectively (Figure 9C and Supplementary Table S3). Furthermore, RBM14 depletion increased the number of telomeres with two or more signals, which is indicative of telomere fragility, with an average of 3.79, 12.47 and 13.52 fragile telomeres per siNT-, siRBM14$^{\#1}$- and siRBM14$^{\#2}$-transfected cell, respectively (Figure 9D and Supplementary Table S3).

Telomere restriction fragment analysis also demonstrated a reduction in the mean length of telomeres following the

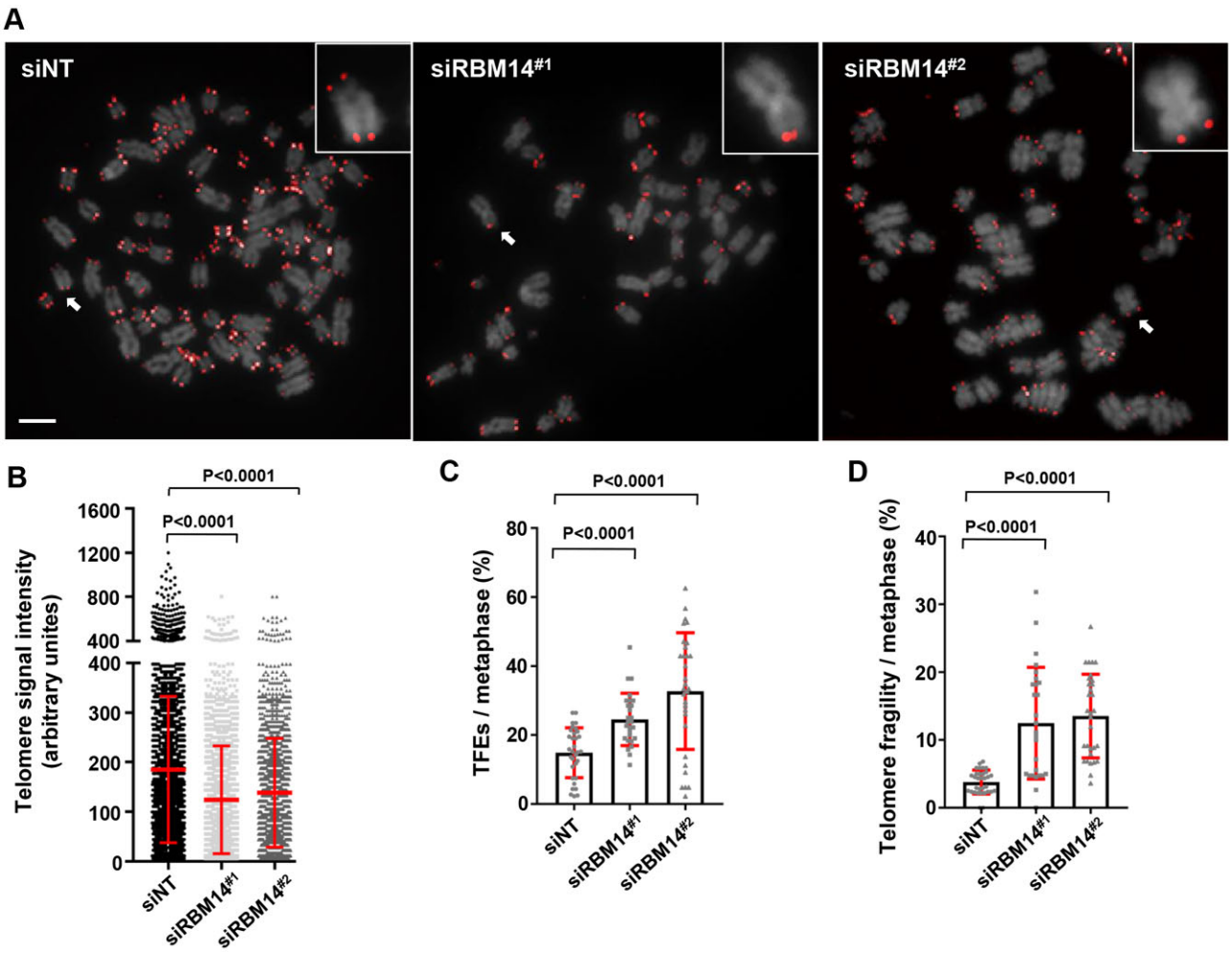

Figure 9. RBM14 depletion leads to telomere loss in ALT cells. (**A**, **B**) Q-FISH analysis of U2OS cells transfected with either non-targeting or RBM14 siRNAs. Representative images show telomere signals (red) and metaphase chromosomes (grey). Insets depict individual chromosomes with (A) or without (B and C) detectable telomere signals. Scale bar: 5 microns. Telomere signal intensities were measured in the indicated U2OS cells. At least 30 metaphases were analyzed per genotype. Each dot represents a single telomere. Red lines depict the mean standard deviation of telomere signal intensities. (**C**, **D**) Quantification of telomere signal-free ends (TFEs)(a chromosome end without detectable telomere signals) and telomere fragility (a telomere chromatid with more than one signal) in the indicated U2OS cells. At least 25 metaphase cells were used to calculate the percentage of TFEs or telomere fragility per metaphase. The data are shown as the mean ± SDs.

depletion of RBM14 (21.6, 19.8 and 19.5 kb in siNT-, siRBM14$^{\#1}$- and siRBM14$^{\#2}$- transfected cell, respectively). Additionally, there was an observed increase in the abundance of smaller telomere restriction fragments in RBM14 knockdown cells. However, ectopic expression of GFP-RBM14 in RBM14 knockdown cells resulted in an increase in the mean telomere length of approximately 22.3 kb, comparable to that observed in the siNT control cells (Supplementary Figure S6). Collectively, our data imply that RBM14 plays an important role in maintaining telomere integrity in ALT cells.

RBM14 depletion leads to a moderate increase in TERRA and R-loops in non-ALT cells

RBM14 was detected at telomeres in HeLa (non-ALT) cells using an isolated chromatin segment approach (55). We confirmed its association with telomeres in HeLa cells by ChIP analysis. Similar to U2OS cells, dot blotting and subsequent hybridization with the Telo-C-Biotin $(CCCTAA)_4$ probe showed that RBM14 and TRF1 immunoprecipitated telomeric DNA; however, IgG did not (Figure 10A).

To determine whether RBM14 modulates telomere maintenance in HeLa cells by regulating TERRA expression and R-loops, RBM14 was depleted from HeLa cells using siRBM14$^{\#1}$ and siRBM14$^{\#2}$ (Figure 10B). RBM14 depletion did not affect total TERRA levels by RNA dot-blot analysis (Figure 10C), but led to moderate increases in some chromosome end-specific TERRA, such as a 1.7-fold increase in 7p by RT-qPCR (Figure 10D and Supplementary Table S3). Our attempts to detect telomeric R-loops by anti-S9.6 DRIP via dot blotting were unsuccessful due to the limited quantity of telomeric R-loops in HeLa cells (56). However, the anti-S9.6 DRIP analysis coupled with telomere qPCR revealed a modest 1.9-fold increase in telomeric R-loops in RBM14 knockdown cells (Figure 10E and Supplementary Table S3).

Intriguingly, Q-FISH analysis revealed that RBM14 depletion did not result in an overall loss of telomere signal, but rather a moderately increased trend in HeLa cells (with an average of 20, 24 and 26 arbitrary units in siNT-, siRBM14$^{\#1}$- and siRBM14$^{\#2}$- transfected cell, respectively)(Figure 10F and Supplementary Table S3). Thus, RBM14 depletion has a mod-

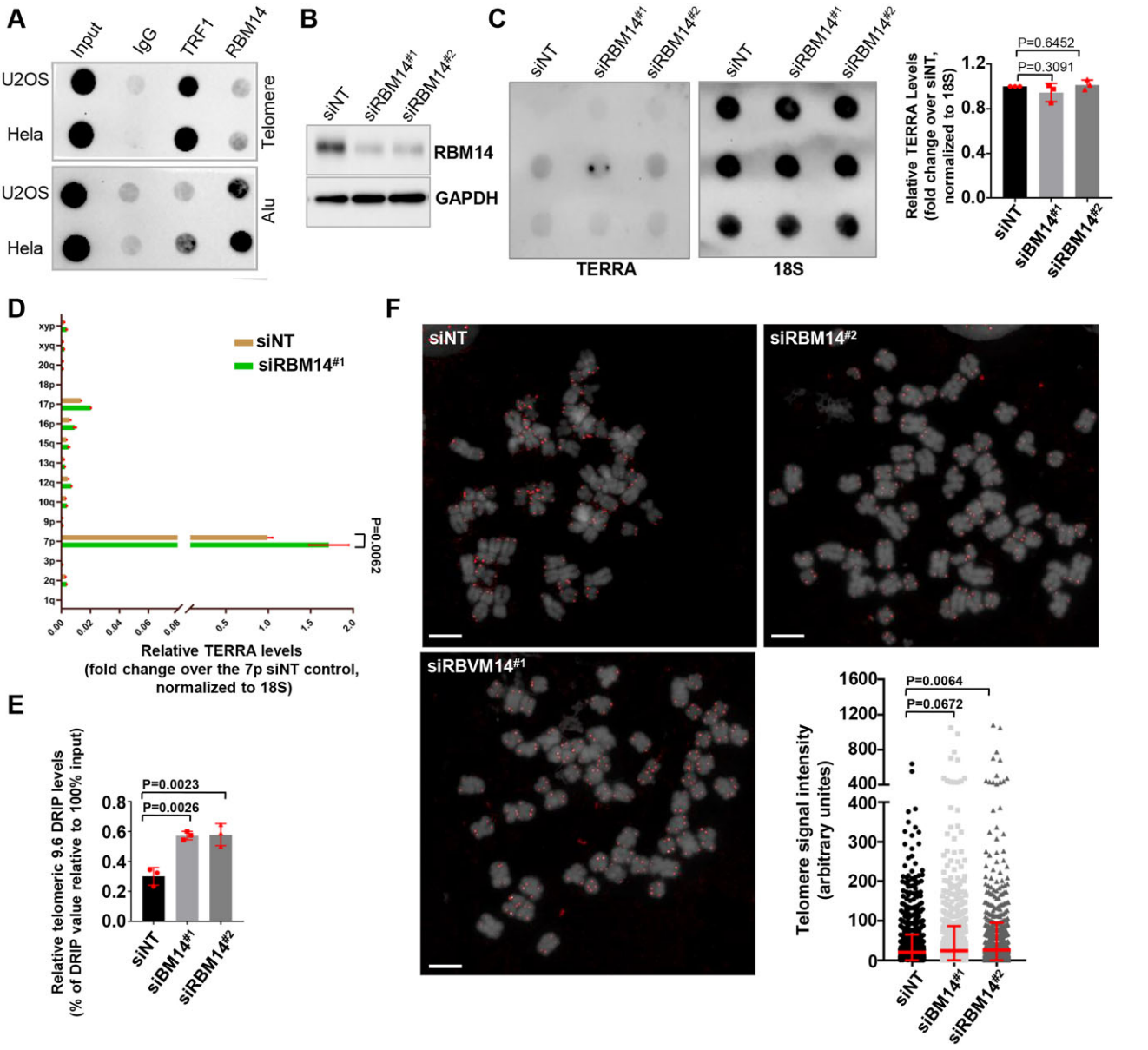

Figure 10. RBM14 depletion leads to a moderate increase in chromosome end TERRA and telomeric R-loops in non-ALT HeLa cells. (**A**) Dot blot analysis of telomere and Alu DNA contents in the indicated ChIP and input from U2OS and HeLa cells using the Telo-C-Biotin $(CCCTAA)_4$ or Alu probes. TRF1 and IgG ChIP served as the positive and negative controls, respectively. (**B**) Western blot analysis of RBM14 in HeLa cells transfected with siNT, siRBM14$^{\#1}$ or siRBM14$^{\#2}$ for 72 h. GAPDH served as the loading control. (**C**) RNA dot blot analysis of total TERRA in HeLa cells transfected with siNT, siRBM14$^{\#1}$ or siRBM14$^{\#2}$ using the Telo-C-Biotin $(CCCTAA)_4$ or 18S probes. The relative TERRA levels were normalized to the values corresponding to 18S and siNT (set to 1) and shown as the mean ± SD of technical triplicates. (**D**) RT-qPCR analysis of chromosome end TERRA in HeLa cells transfected with siNT, siRBM14$^{\#1}$ or siRBM14$^{\#2}$. Relative RT-qPCR values were normalized to the 18S rRNA control. Individual chromosome end-specific TERRA values were further normalized to the 7p siNT control (set to 1). The data were shown as the mean ± SDs of three independent experiments. (**E**) Telomeric R-loop levels in HeLa cells transfected with siNT, siRBM14$^{\#1}$, or siRBM14$^{\#2}$ by telomere qPCR analysis of the S9.6-DRIP. The percentage of DRIP values in the indicated samples were normalized to the values corresponding to 100% input. The bar graph depicts the mean ± SD of three independent experiments. (**F**) Q-FISH analysis of HeLa cells transfected with siNT, siRBM14$^{\#1}$ or siRBM14$^{\#2}$. Representative images show telomere signals (red) and metaphase chromosomes (grey). Telomere signal intensities were measured in the indicated cells. At least 25 metaphases were analyzed per genotype. Each dot represents a single telomere. Red lines depict the mean standard deviation of telomere signal intensities. Scale bar: 5 microns.

erate effect on TERRA, R-loop and telomere maintenance in non-ALT cells.

Discussion

RBM14 is a versatile RNA-binding protein with multiple functions. Previous studies have demonstrated its involvement in NHEJ-mediated DSB repair. In this study, we provide evidence that RBM14 is a telomeric protein that interacts with TERRA and telomeric R-loops. RBM14 is required for the regulation of TERRA levels and the formation of TERRA R-loops at telomeres. This regulatory function of RBM14 contributes to telomere maintenance in human cancer cells.

We have previously reported that RBM14 is recruited to I-PpoI- or microlaser-induced DSBs via a PARP1- and KU-dependent mechanism. This recruitment promotes the NHEJ pathway, which facilitates DSB repair (31). In this study, we demonstrated that RBM14 is localized to telomeres in human cancer cells within the context of normal physiological conditions. Notably, this localization occurs independently of PARP1 and KU, but is subject to the influence of TERRA levels. These findings suggest that RBM14 plays a role in telomeres through its RNA regulatory function, independent of its NHEJ repair function.

A group of RNA-binding proteins bind to TERRA (30,31,51). iDRiP-mass spectrometry identified RBM14 as one of the putative TERRA-binding proteins in ALT cells (30). We validated this interaction and investigated its function in telomere maintenance in human cancer cells, with a focus on ALT cells, because TERRA and TERRA R-loops play critical roles in ALT telomeres. We observed that RBM14 modulates TERRA levels, and its depletion increased both total and chromosome end-specific TERRA levels. As RBM14 exerts inhibitory effects on transcription (57), we investigated its involvement in the regulation of chromatin architecture at the 10q and 13q subtelomeric loci, which have been shown to influence TERRA expression (48). Indeed, RBM14 exhibits binding affinity towards the subtelomeres located at 10q and 13q, and its absence influences the occupancy of RNAPII, H3K4me3 and H3K9me3 at these subtelomeric loci. Moreover, our data indicate that the increased levels of TERRA in cells with depleted RBM14 may be a result of an extended half-life and/or a decreased rate of TERRA RNA degradation. Thus, it is conceivable that the increase in TERRA transcription, the prolongation of TERRA half-life, or a combination of both mechanisms contribute to the increase in TERRA after RBM14 depletion.

The ability of TERRA to generate R-loops at telomeres is regulated by its level of expression and interactions with telomeric proteins and DNA repair proteins (58). In this study, we revealed that RBM14 has a direct, dose-dependent binding affinity for TERRA *in vitro*, as well as an *in vivo* interaction between RBM14 and TERRA. Furthermore, the interaction between RBM14 and TERRA results in a reduced capacity of TERRA to form R-loop structures with DNA oligonucleotides *in vitro*. RBM14 has previously been shown to bind to genomic R-loops in human cells (35). Our ChIP-reChIP analysis in this study demonstrated that RBM14 interacts with telomeric R-loops in ALT cells, while RBM14 depletion increased the frequency of R-loops at telomeres. These findings indicate that RBM14 has a direct affinity for TERRA, inhibiting it from being integrated into telomeric R-loops. This is in contrast to TRF2, which has been shown to bind to TERRA and promote the formation of TERRA R-loops (27).

Although telomeric R-loops help to maintain telomeres, an excess of them may impede DNA replication, resulting in telomere replication stress or collapse, telomere strand breakage and telomere loss (21,23–25,59–61). Several lines of evidence indicate that this possibility may have occurred following the depletion of RBM14. First, RBM14 deficiency increased R-loop levels at telomeres. Second, RBM14 deficiency increased the formation of telomere dysfunction-induced DNA damage foci (or TIFs), which was exacerbated by low-dose aphidicolin. Third, RBM14 deficiency led to an accumulation of the phosphorylated ssDNA-binding protein RPA32 (pSer33) at telomeres. Fourth, TIFs and telomeric RPA32 (pSer33) were less abundant in RBM14 deficient cells following RNase H1 treatment. Lastly, RBM14 deficiency had a detrimental impact on both the length and integrity of telomeres. As a result, RBM14 may modulate the equilibrium of R-loop levels to ensure unimpeded replication and maintenance of telomeres in ALT cells.

Our study also provides evidence that RBM14 exerts a moderate regulatory effect on TERRA and telomeric R-loops in non-ALT HeLa cells, although RBM14 did not result in telomere shortening as observed in ALT cells. The observed disparity in telomere length phenotype between telomerase-positive and ALT cancer cells can be attributed to a number of factors, including variations in TERRA and R-loop levels within these cancer cells (20,21,62–65). In ALT cancer cells, TERRA and telomeric R-loops are prevalent, and further elevation of TERRA and telomeric R-loops by RBM14 depletion may result in the collapse of DNA replication and the subsequent loss of telomeres. In contrast, TERRA and telomeric R-loops in telomerase-positive cells is tightly controlled. A modest augmentation of TERRA R-loops may contribute to the preservation of telomeres by regulating telomerase, HR proteins and chromatin modifiers, particularly in situations where telomeres are subjected to damage or reach a critically shortened state (56).

Based on our findings, it is posited that RBM14 modulates TERRA levels and impedes the formation of TERRA R-loops at telomeres. RBM14 deficiency results in the accumulation of TERRA and telomeric R-loops, thereby affecting the equilibrium of telomere length in human cancer cells (Supplementary Figure S7). Because of its ability to preserve telomere integrity in human cancer cells, RBM14 represents a novel telomere regulator. Understanding the function of RBM14 at telomeres is likely to yield novel insights into telomere maintenance pathways and therapeutic avenues.

Data availability

The data underlying this article are available in the article and in its online supplementary material. Further data underlying this article will be shared on reasonable request to the corresponding author.

Supplementary data

Supplementary Data are available at NAR Online.

Acknowledgements

We sincerely thank Dr Claus M. Azzalin for his invaluable guidance and for generously providing us with the TERRA detection protocols, and Mr. Marc Raley for assistance with the illustrations.

Author contributions: Y.L. conceived the project. Y.W. and Y.L. designed the experiments. Y.W., W.Z., Y.J., J.A.S., Y.G., C.P., D.L.C., M.K. and Y.L. performed experiments, statistical analysis and/or data analysis; Y.L., Y.Y. and M.K. provided project administration, resource and supervision support. Y.L. and Y.W. wrote the manuscript, and all authors read, reviewed and/or edited the manuscript.

Funding

Intramural Research Program of the National Institute on Aging. Funding for open access charge: Intramural Research Program of the National Institute on Aging.

Conflict of interest statement

None declared.

References

1. de Lange,T. (2018) Shelterin-mediated telomere protection. *Annu. Rev. Genet*, **52**, 223–247.
2. O'sullivan,R.J. and Karlseder,J. (2010) Telomeres: protecting chromosomes against genome instability. *Nat. Rev. Mol. Cell Biol.*, **11**, 171–181.
3. d'Adda di Fagagna,F., Teo,S.H. and Jackson,S.P. (2004) Functional links between telomeres and proteins of the DNA-damage response. *Genes Dev.*, **18**, 1781–1799.
4. Bryan,T.M., Englezou,A., Dalla-Pozza,L., Dunham,M.A. and Reddel,R.R. (1997) Evidence for an alternative mechanism for maintaining telomere length in human tumors and tumor-derived cell lines. *Nat. Med.*, **3**, 1271–1274.
5. Dilley,R.L., Verma,P., Cho,N.W., Winters,H.D., Wondisford,A.R. and Greenberg,R.A. (2016) Break-induced telomere synthesis underlies alternative telomere maintenance. *Nature*, **539**, 54–58.
6. Zhang,J.-M., Yadav,T., Ouyang,J., Lan,L. and Zou,L. (2019) Alternative lengthening of telomeres through two distinct break-induced replication pathways. *Cell Rep.*, **26**, 955–968.
7. Cesare,A.J. and Reddel,R.R. (2010) Alternative lengthening of telomeres: models, mechanisms and implications. *Nat. Rev. Genet.*, **11**, 319–330.
8. Bonnell,E., Pasquier,E. and Wellinger,R.J. (2021) Telomere replication: solving multiple end replication problems. *Front. Cell Dev. Biol.*, **9**, 668171.
9. Gilson,E. and Geli,V. (2007) How telomeres are replicated. *Nat. Rev. Mol. Cell Biol.*, **8**, 825–838.
10. Azzalin,C.M., Reichenbach,P., Khoriauli,L., Giulotto,E. and Lingner,J. (2007) Telomeric repeat–containing RNA and RNA surveillance factors at mammalian chromosome ends. *Science*, **318**, 798–801.
11. Schoeftner,S. and Blasco,M.A. (2008) Developmentally regulated transcription of mammalian telomeres by DNA-dependent RNA polymerase II. *Nat. Cell Biol.*, **10**, 228–236.
12. Luke,B., Panza,A., Redon,S., Iglesias,N., Li,Z. and Lingner,J. (2008) The Rat1p 5' to 3' exonuclease degrades telomeric repeat-containing RNA and promotes telomere elongation in Saccharomyces cerevisiae. *Mol. Cell*, **32**, 465–477.
13. Bah,A., Wischnewski,H., Shchepachev,V. and Azzalin,C.M. (2012) The telomeric transcriptome of Schizosaccharomyces pombe. *Nucleic Acids Res.*, **40**, 2995–3005.
14. Vrbsky,J., Akimcheva,S., Watson,J.M., Turner,T.L., Daxinger,L., Vyskot,B., Aufsatz,W. and Riha,K. (2010) siRNA-mediated methylation of Arabidopsis telomeres. *PLoS Genet.*, **6**, e1000986.
15. Rudenko,G. and Van der Ploeg,L.H. (1989) Transcription of telomere repeats in protozoa. *EMBO J.*, **8**, 2633–2638.
16. Nergadze,S.G., Farnung,B.O., Wischnewski,H., Khoriauli,L., Vitelli,V., Chawla,R., Giulotto,E. and Azzalin,C.M. (2009) CpG-island promoters drive transcription of human telomeres. *RNA*, **15**, 2186–2194.
17. Diman,A. and Decottignies,A. (2018) Genomic origin and nuclear localization of TERRA telomeric repeat-containing RNA: from Darkness to Dawn. *FEBS J.*, **285**, 1389–1398.
18. Feuerhahn,S., Iglesias,N., Panza,A., Porro,A. and Lingner,J. (2010) TERRA biogenesis, turnover and implications for function. *FEBS Lett.*, **584**, 3812–3818.
19. Perez-Martinez,L., Wagner,T. and Luke,B. (2022) Telomere Interacting Proteins and TERRA Regulation. *Front. Genet.*, **13**, 872636.
20. Arora,R., Lee,Y., Wischnewski,H., Brun,C.M., Schwarz,T. and Azzalin,C.M. (2014) RNaseH1 regulates TERRA-telomeric DNA hybrids and telomere maintenance in ALT tumour cells. *Nat. Commun.*, **5**, 1–11.
21. Fernandes,R.V., Feretzaki,M. and Lingner,J. (2021) The makings of TERRA R-loops at chromosome ends. *Cell Cycle*, **20**, 1745–1759.
22. Graf,M., Bonetti,D., Lockhart,A., Serhal,K., Kellner,V., Maicher,A., Jolivet,P., Teixeira,M.T. and Luke,B. (2017) Telomere length determines TERRA and R-loop regulation through the cell cycle. *Cell*, **170**, 72–85.
23. Balk,B., Maicher,A., Dees,M., Klermund,J., Luke-Glaser,S., Bender,K. and Luke,B. (2013) Telomeric RNA-DNA hybrids affect telomere-length dynamics and senescence. *Nat. Struct. Mol. Biol.*, **20**, 1199–1205.
24. Brickner,J.R., Garzon,J.L. and Cimprich,K.A. (2022) Walking a tightrope: the complex balancing act of R-loops in genome stability. *Mol. Cell*, **82**, 2267–2297.
25. Pfeiffer,V., Crittin,J., Grolimund,L. and Lingner,J. (2013) The THO complex component Thp2 counteracts telomeric R-loops and telomere shortening. *EMBO J.*, **32**, 2861–2871.
26. Cusanelli,E. and Chartrand,P. (2015) Telomeric repeat-containing RNA TERRA: a noncoding RNA connecting telomere biology to genome integrity. *Front. Genet.*, **6**, 143.
27. Lee,Y.W., Arora,R., Wischnewski,H. and Azzalin,C.M. (2018) TRF1 participates in chromosome end protection by averting TRF2-dependent telomeric R loops. *Nat. Struct. Mol. Biol.*, **25**, 147–153.
28. Mei,Y., Deng,Z., Vladimirova,O., Gulve,N., Johnson,F.B., Drosopoulos,W.C., Schildkraut,C.L. and Lieberman,P.M. (2021) TERRA G-quadruplex RNA interaction with TRF2 GAR domain is required for telomere integrity. *Sci. Rep.*, **11**, 1–14.
29. Deng,Z., Norseen,J., Wiedmer,A., Riethman,H. and Lieberman,P.M. (2009) TERRA RNA binding to TRF2 facilitates heterochromatin formation and ORC recruitment at telomeres. *Mol. Cell*, **35**, 403–413.
30. Chu,H.-P., Cifuentes-Rojas,C., Kesner,B., Aeby,E., Lee,H., Wei,C., Oh,H.J., Boukhali,M., Haas,W. and Lee,J.T. (2017) TERRA RNA antagonizes ATRX and protects telomeres. *Cell*, **170**, 86–101.
31. Jang,Y., Elsayed,Z., Eki,R., He,S., Du,K.-P., Abbas,T. and Kai,M. (2020) Intrinsically disordered protein RBM14 plays a role in generation of RNA: DNA hybrids at double-strand break sites. *Proc. Natl. Acad. Sci.*, **117**, 5329–5338.
32. Simon,N.E., Yuan,M. and Kai,M. (2017) RNA-binding protein RBM14 regulates dissociation and association of non-homologous end joining proteins. *Cell Cycle*, **16**, 1175–1180.
33. Kai,M. (2016) Roles of RNA-binding proteins in DNA damage response. *Int. J. Mol. Sci.*, **17**, 310.
34. Auboeuf,D., Dowhan,D.H., Li,X., Larkin,K., Ko,L., Berget,S.M. and O'Malley,B.W. (2004) CoAA, a nuclear receptor coactivator protein at the interface of transcriptional coactivation and RNA splicing. *Mol. Cell. Biol.*, **24**, 442–453.

35. Wang,I.X., Grunseich,C., Fox,J., Burdick,J., Zhu,Z., Ravazian,N., Hafner,M. and Cheung,V.G. (2018) Human proteins that interact with RNA/DNA hybrids. *Genome Res.*, **28**, 1405–1414.
36. Vohhodina,J., Goehring,L.J., Liu,B., Kong,Q., Botchkarev Jr,V.V., Huynh,M., Liu,Z., Abderazzaq,F.O., Clark,A.P. and Ficarro,S.B. (2021) BRCA1 binds TERRA RNA and suppresses R-Loop-based telomeric DNA damage. *Nat. Commun.*, **12**, 1–16.
37. Barski,A., Cuddapah,S., Cui,K., Roh,T.-Y., Schones,D.E., Wang,Z., Wei,G., Chepelev,I. and Zhao,K. (2007) High-resolution profiling of histone methylations in the human genome. *Cell*, **129**, 823–837.
38. Furlan-Magaril,M., Rincon-Arano,H. and Recillas-Targa,F. (2009) Sequential chromatin immunoprecipitation protocol: chIP-reChIP. *Methods Mol. Biol.*, **543**, 253–266.
39. Sun,C., Wang,K., Stock,A.J., Gong,Y., Demarest,T.G., Yang,B., Giri,N., Harrington,L., Alter,B.P., Savage,S.A., *et al.* (2020) Re-equilibration of imbalanced NAD metabolism ameliorates the impact of telomere dysfunction. *EMBO J.*, **39**, e103420.
40. Feretzaki,M. and Lingner,J. (2017) A practical qPCR approach to detect TERRA, the elusive telomeric repeat-containing RNA. *Methods*, **114**, 39–45.
41. Dimitrova,N. and de Lange,T. (2006) MDC1 accelerates nonhomologous end-joining of dysfunctional telomeres. *Genes Dev.*, **20**, 3238–3243.
42. Wang,Y., Ferrucci,L., Seidman,M.M. and Liu,Y. (2022) An optimized proximity ligation assay to detect telomere dysfunction induced foci in human and mouse cells. *STAR Protoc*, **3**, 101610.
43. Wan,B., Yin,J., Horvath,K., Sarkar,J., Chen,Y., Wu,J., Wan,K., Lu,J., Gu,P. and Yu,E.Y. (2013) SLX4 assembles a telomere maintenance toolkit by bridging multiple endonucleases with telomeres. *Cell Rep.*, **4**, 861–869.
44. Silva,B., Pentz,R., Figueira,A.M., Arora,R., Lee,Y.W., Hodson,C., Wischnewski,H., Deans,A.J. and Azzalin,C.M. (2019) FANCM limits ALT activity by restricting telomeric replication stress induced by deregulated BLM and R-loops. *Nat. Commun.*, **10**, 1–16.
45. Mersaoui,S.Y., Yu,Z., Coulombe,Y., Karam,M., Busatto,F.F., Masson,J.Y. and Richard,S. (2019) Arginine methylation of the DDX5 helicase RGG/RG motif by PRMT5 regulates resolution of RNA:DNA hybrids. *EMBO J.*, **38**, e100986.
46. Sarkar,J., Wan,B., Yin,J., Vallabhaneni,H., Horvath,K., Kulikowicz,T., Bohr,V.A., Zhang,Y., Lei,M. and Liu,Y. (2015) SLX4 contributes to telomere preservation and regulated processing of telomeric joint molecule intermediates. *Nucleic Acids Res.*, **43**, 5912–5923.
47. Biffi,G., Tannahill,D. and Balasubramanian,S. (2012) An intramolecular G-quadruplex structure is required for binding of telomeric repeat-containing RNA to the telomeric protein TRF2. *J. Am. Chem. Soc.*, **134**, 11974–11976.
48. Deng,Z., Wang,Z., Stong,N., Plasschaert,R., Moczan,A., Chen,H.S., Hu,S., Wikramasinghe,P., Davuluri,R.V. and Bartolomei,M.S. (2012) A role for CTCF and cohesin in subtelomere chromatin organization, TERRA transcription, and telomere end protection. *EMBO J.*, **31**, 4165–4178.
49. Chedin,F., Hartono,S.R., Sanz,L.A. and Vanoosthuyse,V. (2021) Best practices for the visualization, mapping, and manipulation of R-loops. *EMBO J.*, **40**, e106394.
50. Grunseich,C., Wang,I.X., Watts,J.A., Burdick,J.T., Guber,R.D., Zhu,Z., Bruzel,A., Lanman,T., Chen,K., Schindler,A.B., *et al.* (2018) Senataxin Mutation Reveals How R-Loops Promote Transcription by Blocking DNA Methylation at Gene Promoters. *Mol. Cell*, **69**, 426–437.
51. Chawla,R., Redon,S., Raftopoulou,C., Wischnewski,H., Gagos,S. and Azzalin,C.M. (2011) Human UPF1 interacts with TPP1 and telomerase and sustains telomere leading-strand replication. *EMBO J.*, **30**, 4047–4058.
52. Crossley,M.P., Bocek,M. and Cimprich,K.A. (2019) R-loops as cellular regulators and genomic threats. *Mol. Cell*, **73**, 398–411.
53. D'Adda di Fagagna,F., Reaper,P.M., Clay-Farrace,L., Fiegler,H., Carr,P., Von Zglinicki,T., Saretzki,G., Carter,N.P. and Jackson,S.P. (2003) A DNA damage checkpoint response in telomere-initiated senescence. *Nature*, **426**, 194–198.
54. Takai,H., Smogorzewska,A. and de Lange,T. (2003) DNA damage foci at dysfunctional telomeres. *Curr. Biol.*, **13**, 1549–1556.
55. Déjardin,J. and Kingston,R.E. (2009) Purification of proteins associated with specific genomic Loci. *Cell*, **136**, 175–186.
56. Feretzaki,M., Pospisilova,M., Valador Fernandes,R., Lunardi,T., Krejci,L. and Lingner,J. (2020) RAD51-dependent recruitment of TERRA lncRNA to telomeres through R-loops. *Nature*, **587**, 303–308.
57. Li,X., Hoeppner,L.H., Jensen,E.D., Gopalakrishnan,R. and Westendorf,J.J. (2009) Co-activator activator (CoAA) prevents the transcriptional activity of Runt domain transcription factors. *J. Cell. Biochem.*, **108**, 378–387.
58. Bettin,N., Oss Pegorar,C. and Cusanelli,E. (2019) The emerging roles of TERRA in telomere maintenance and genome stability. *Cells*, **8**, 246.
59. Aguilera,A. and García-Muse,T. (2012) R loops: from transcription byproducts to threats to genome stability. *Mol. Cell*, **46**, 115–124.
60. Bermejo,R., Lai,M.S. and Foiani,M. (2012) Preventing replication stress to maintain genome stability: resolving conflicts between replication and transcription. *Mol. Cell*, **45**, 710–718.
61. Santos-Pereira,J.M. and Aguilera,A. (2015) R loops: new modulators of genome dynamics and function. *Nat. Rev. Genet.*, **16**, 583–597.
62. Episkopou,H., Draskovic,I., Van Beneden,A., Tilman,G., Mattiussi,M., Gobin,M., Arnoult,N., Londono-Vallejo,A. and Decottignies,A. (2014) Alternative Lengthening of Telomeres is characterized by reduced compaction of telomeric chromatin. *Nucleic Acids Res.*, **42**, 4391–4405.
63. Flynn,R.L., Cox,K.E., Jeitany,M., Wakimoto,H., Bryll,A.R., Ganem,N.J., Bersani,F., Pineda,J.R., Suva,M.L., Benes,C.H., *et al.* (2015) Alternative lengthening of telomeres renders cancer cells hypersensitive to ATR inhibitors. *Science*, **347**, 273–277.
64. Ng,L.J., Cropley,J.E., Pickett,H.A., Reddel,R.R. and Suter,C.M. (2009) Telomerase activity is associated with an increase in DNA methylation at the proximal subtelomere and a reduction in telomeric transcription. *Nucleic Acids Res.*, **37**, 1152–1159.
65. Gong,Y. and Liu,Y. (2023) R-loops at chromosome ends: from formation, regulation, and cellular consequence. *Cancers (Basel)*, **15**, 2178.

Received: February 9, 2023. **Editorial Decision:** October 3, 2023. **Accepted:** October 13, 2023